สภาพเข้ากันได้ของขั้วแคโทดเพอรอฟสไกต์ $(Ba_{0.5}Sr_{0.5})_{0.7}Ca_{0.3}Co_{0.8}Fe_{0.2}O_{3-\delta}$ กับอิเล็กโทรไลต์ YSZ สำหรับเซลล์เชื้อเพลิงออกไซด์ของแข็ง

นางสาววิชุมา จิราโรจน์

วิทยานิพนธ์นี้เป็นส่วนหนึ่งของการศึกษาตามหลักสูตรปริญญาวิทยาศาสตรมหาบัณฑิต
สาขาวิชาเคมี ภาควิชาเคมี
คณะวิทยาศาสตร์ จุฬาลงกรณ์มหาวิทยาลัย
ปีการศึกษา 2556

COMPATIBILITY OF $(Ba_{0.5}Sr_{0.5})_{0.7}Ca_{0.3}Co_{0.8}Fe_{0.2}O_{3-\delta}$ PEROVSKITE CATHODE AND YSZ ELECTROLYTE FOR SOLID OXIDE FUEL CELL

Miss Wichuma Jiraroj

A Thesis Submitted in Partial Fulfillment of the Requirements
for the Degree of Master of Science Program in Chemistry
Department of Chemistry
Faculty of Science
Chulalongkorn University
Academic Year 2013

Thesis Title	COMPATIBILITY OF $(Ba_{0.5}Sr_{0.5})_{0.7}Ca_{0.3}Co_{0.8}Fe_{0.2}O_{3-\delta}$ PEROVSKITE CATHODE AND YSZ ELECTROLYTE FOR SOLID OXIDE FUEL CELL
By	Miss Wichuma Jiraroj
Field of Study	Chemistry
Thesis Advisor	Assistant Professor Soamwadee Chaianansutcharit, Ph.D.
Thesis Co-Advisor	Parichatr Vanalabhpatana, Ph.D.

Accepted by the Faculty of Science, Chulalongkorn University in Partial Fulfillment of the Requirements for the Master's Degree

.....Dean of the Faculty of Science

(Professor Supot Hannongbua, Dr.rer.nat.)

THESIS COMMITTEE

.....Chairman

(Assistant Professor Warinthorn Chavasiri, Ph.D.)

.....Thesis Advisor

(Assistant Professor Soamwadee Chaianansutcharit, Ph.D.)

.....Thesis Co-Advisor

(Parichatr Vanalabhpatana, Ph.D.)

.....Examiner

(Assistant Professor Boosayarat Tomapatanaget, Ph.D.)

.....External Examiner

(Siriporn Larpkeattavorn, Ph.D.)

วิชุมา จิราโรจน์ : สภาพเข้ากันได้ของขั้วแคโทดเพอรอฟสไกต์ $(Ba_{0.5}Sr_{0.5})_{0.7}Ca_{0.3}Co_{0.8}Fe_{0.2}O_{3-\delta}$ กับอิเล็กโทรไลต์ YSZ สำหรับเซลล์เชื้อเพลิงออกไซด์ของแข็ง. (COMPATIBILITY OF $(Ba_{0.5}Sr_{0.5})_{0.7}Ca_{0.3}Co_{0.8}Fe_{0.2}O_{3-\delta}$ PEROVSKITE CATHODE AND YSZ ELECTROLYTE FOR SOLID OXIDE FUEL CELL) อ.ที่ปรึกษาวิทยานิพนธ์หลัก: ผศ. ดร.โสมวดี ไชยอนันต์สุจริต, อ.ที่ปรึกษาวิทยานิพนธ์ร่วม: อ. ดร. ปาริฉัตร วนลาภพัฒนา, 68 หน้า.

ศึกษาสารประกอบคอมพอสิตระหว่าง $(Ba_{0.5}Sr_{0.5})_{0.7}Ca_{0.3}Co_{0.8}Fe_{0.2}O_{3-\delta}$ กับสารอิเล็กโทรไลต์ YSZ และ GDC ในอัตรส่วน 3:1, 1:1 และ 1:3 โดยน้ำหนัก ที่อุณหภูมิ 850 -1300 องศาเซลเซียส ตรวจสอบเอกลักษณ์ของสารประกอบคอมพอสิตด้วยเทคนิค XRD โครงสร้างของ $Sr(ZrO_3)$, $SrCoO_3$ and $CaZrO_3$ ปรากฏขึ้นเมื่อเผา BSCCF:YSZ ที่อุณหภูมิ 850 - 1300 องศาเซลเซียส เป็นเวลา 7-9 ชั่วโมง ในขณะที่เผาสารประกอบคอมพอสิต BSCCF:GDC ที่อุณหภูมิ 850 องศาเซลเซียสจะไม่พบโครงดังกล่าว วัดการนำไฟฟ้าและการซึมผ่านออกซิเจนของสารประกอบคอมโพสิตทั้งสองชนิดพบว่ามีค่าต่ำกว่าค่าการนำไฟฟ้าและอัตราการซึมผ่านออกซิเจนของ $(Ba_{0.5}Sr_{0.5})_{0.7}Ca_{0.3}Co_{0.8}Fe_{0.2}O_{3-\delta}$ จากนั้นศึกษาความต้านทานของแผ่นเซลล์สมมาตร และสมรรถนะเซลล์เดี่ยวของ $(Ba_{0.5}Sr_{0.5})_{0.7}Ca_{0.3}Co_{0.8}Fe_{0.2}O_{3-\delta}$ และสารประกอบคอมพอสิตที่อุณหภูมิ 850–650 องศาเซลเซียส พบว่าเซลล์สมมาตรและเซลล์เดี่ยวของ $(Ba_{0.5}Sr_{0.5})_{0.7}Ca_{0.3}Co_{0.8}Fe_{0.2}O_{3-\delta}$ ที่ขึ้นรูปโดยมี GDC เป็นอินเตอร์เลเยอร์ให้ค่าความต้านทานต่ำสุด และให้ค่าสมรรถนะเซลล์เดี่ยวสูงที่สุดประมาณ 163.84 มิลลิวัตต์ต่อตารางเซนติเมตร ที่อุณหภูมิ 850 องศาเซลเซียส ตรวจสอบลักษณะพื้นผิวของและภาพตัดขวางของแคโทดภายหลังการทดสอบสมรรถนะเซลล์เดี่ยวพบว่าไม่มีการเปลี่ยนแปลงสภาพในเซลล์เดี่ยวที่มี GDC เป็นอินเตอร์เลเยอร์

ภาควิชา เคมี ลายมือชื่อนิสิต .....

สาขาวิชา เคมี ลายมือชื่อ อ.ที่ปรึกษาวิทยานิพนธ์หลัก .....

ปีการศึกษา 2556 ลายมือชื่อ อ.ที่ปรึกษาวิทยานิพนธ์ร่วม .....

5372329023 : MAJOR CHEMISTRY
KEYWORDS: IMPEDANCE / PEROVSKITE / POWER DENSITY / SOLID OXIDE FUEL CELL / COMPOSITE

WICHUMA JIRAROJ: COMPATIBILITY OF $(Ba_{0.5}Sr_{0.5})_{0.7}Ca_{0.3}Co_{0.8}Fe_{0.2}O_{3-\delta}$ PEROVSKITE CATHODE AND YSZ ELECTROLYTE FOR SOLID OXIDE FUEL CELL. ADVISOR: ASST. PROF. SOAMWADEE CHAIANANSUTCHARIT, Ph.D., CO-ADVISOR: PARICHATR VANALABHPATANA, Ph.D., 68pp.

The composites of $(Ba_{0.5}Sr_{0.5})_{0.7}Ca_{0.3}Co_{0.8}Fe_{0.2}O_{3-\delta}$ (BSCCF) with YSZ and GDC electrolytes in 1:3, 1:1 and 3:1 weight ratio were investigated at 850 – 1300 °C. Phase structures were characterized by XRD. $Sr(ZrO_3)$, $SrCoO_3$ and $CaZrO_3$ were obtained after firing the BSCCF:YSC composites at 850 -1300 °C for 7-10 hrs, on the contary no other phases were observed when the BSCCF:GDC composites were fired at 850 °C. The electrical conductivity and the oxygen permeation of both composites were lower than $(Ba_{0.5}Sr_{0.5})_{0.7}Ca_{0.3}Co_{0.8}Fe_{0.2}O_{3-\delta}$. The internal resistance of symmetric cell and the single cell performance of $(Ba_{0.5}Sr_{0.5})_{0.7}Ca_{0.3}Co_{0.8}Fe_{0.2}O_{3-\delta}$ and composites were performed at 850 – 650 °C. It was found that the symmetric cell of $(Ba_{0.5}Sr_{0.5})_{0.7}Ca_{0.3}Co_{0.8}Fe_{0.2}O_{3-\delta}$ fabricated with the GDC interlayer showed the lowest interfacial resistance at 850 °C. And, the highest single cell performance was obtained from $(Ba_{0.5}Sr_{0.5})_{0.7}Ca_{0.3}Co_{0.8}Fe_{0.2}O_{3-\delta}$ with the GDC interlayer as 163.84 mW/cm^2 at 850 °C. Surface morphology and cross section images of cathodes after the single cell performance indicated no transformation of cathode along the interface on the single cell coated with GDC interlayer.

Department:	Chemistry	Student's Signature	.....
Field of Study:	Chemistry	Advisor's Signature	.....
Academic Year:	2013	Co-Advisor's Signature	.....

ACKNOWLEDGEMENTS

The achivement of this thesis can be attributed to the extensive support and assistance from Assistant Professor Dr. Soamwadee Chaianunsutcharit, author's advisor and Dr. Parichatr Vanalabpatana, co-advisor. The author also deeply shows gratitude to her valuable advices, guidance and experiment supporting for this research. Moreover, the author is deeply appreciate to Professor Dr. Kazunari Sato, Nagaoka University of Technology, Japan, exchange program advisor for his kindness and valuable advices.

In addition, the author wishes to send a deeply grateful to Assistant Professor Dr. Warinthorn Chavasiri, Assistant Professor Dr. Boosayarat Tomapatanaget and Dr. Siriporn Larpkeattavorn for serving as the chairman and members of this thesis committee, respectively, for their valuable suggestions and comments.

The authors gratefully acknowledge financial support of student exchange grant from JASSO scholarship program 2011, Nagaoka University of Technology, Japan. Afterwards, the author would like to thank Materials Chemistry and Catalysis Research Unit (MATCAT) for provision of experimental facilities. Acknowledgement is also extended to Department of Chemistry, Faculty of Science, Chulalongkorn University for granting financial support to fulfill this study.

This thesis cannot be complete without generous help of the members of Materials Chemistry and Catalysis Research Unit (MATCAT) and laboratory at Nagaoka University of Technology. Special thank is also express them for their kindness, advices and encouragement.

Finally, the author would like forward the deepest gratitude to the author's family for their entirely care and encouragement.

CONTENTS

Page

Page

Page

LIST OF TABLES

Table **Page**

LIST OF FIGURES

Figure **Page**

LIST OF ABBREVIATIONS

SOFC	Solid Oxide Fuel Cell
XRD	X-ray diffractrometer
SEM	Scanning electron microscopy
EPMA	Electron probe microanalysis
hrs	Hours
wt%	Percent by weight
K	Kelvin
°C	Degree Celsius
YSZ	Yiitria stabilized Zirconia
GDC	Galdolinia doped ceria
LSM	Perovskite containing La, Sr and Mn
BSCCF	Perovskite containing Ba, Sr, Ca, Co and Fe

CHAPTER I
INTRODUCTION

1.1 Background

Nowadays, fossil fuels such as coal, petroleum and oil shale are commonly popular for generating electricity. They are non-renewable energy sources which cannot be regrown, regenerated, or reproduced on a scale in order to sustain the consumption rate. Fossil fuels can emit hazardous chemicals e.g. SO_2, NO_2 and CO_2 which are causes of acid rain and greenhouse effect, from the combustion [1, 2]. Therefore, scientists consider to find alternative energy sources which are non-polluting i.e. wind power, solar cell, biomass and fuel cell [3]. A fuel cell is an electrochemical device which converts oxygen and hydrogen into electricity. Water and heat produced as by-products of the fuel cell can be used in the hydrogen fuel cell and electrical equipments respectively.

Solid oxide fuel cells (SOFCs) [4] are of interested because of their high-efficiency in energy conversion, low pollution emission and efficient waste-heat utilization. SOFC device can promote the efficiency as high as 65% and the flexibility of fuel such as hydrogen gas, methane and alcohol is previlage. The most prevalent materials in SOFCs are yttria-stabillized zirconia (YSZ) as an electrolyte, nickel-YSZ as an anode and strontium-doped lanthanum manganite (LSM) as a cathode.

1.2 Literature reviews

1.2.1 Literature reviews of cathode materials

The cathode is an important part of solid oxide fuel cell components. The cathodes material should release high electro catalytic of oxygen reduction and high electrical conductivity.[5] The commonly used cathode in solid oxide fuel cells is perovskite especially Sr-doped lanthanum manganite. However, Sr-doped lanthanum manganite is extremely low oxygen ion conductivity that limits the O_2 reduction

reactions at intermediate-temperatures range (600–750°C). Consequently, the development of a new cathode material for a good performance at low operation temperatures has gained much attention such as $Ba_{0.5}Sr_{0.5}Co_{0.8}Fe_{0.2}O_{3-\delta}$, $L_{0.5}Sr_{0.5}Co_{0.8}Fe_{0.2}O_{3-\delta}$ and $La_{0.5}Sr_{1.5}CoO_4$. $Ba_{0.5}Sr_{0.5}Co_{0.8}Fe_{0.2}O_{3-\delta}$ (BSCF) perovskite has been reported by Shao and Haile [6] as a new cathode material for reducing the operating temperature of SOFC and exhibiting the high power densities at 500 – 600°C. A single cell, $Ba_{0.5}Sr_{0.5}Co_{0.8}Fe_{0.2}O_{3-\delta}$ I $Sm_{0.15}Ce_{0.85}O_{2-\delta}$ I Ni-$Sm_{0.15}Ce_{0.85}O_{2-\delta}$ was investigated and the maximum power densities were obtained 1,010 mW/cm^2 at 600°C and 402mW/cm^2 and 500°C . However, BSCF cathode is a mixed ionic and electronic conductor (MIEC) with high oxygen ion permeability but low electrical conductivity (50 S/cm at 392°C); thus BSCF has been developed in many ways e.g. increasing of charge carrier, the substituting ions at the A-site, etc. Suwicha *et al*. [7] was successfully improved an electrical conductivity of BSCF by substitution Ca ion in A-site. The maximum electrical conductivity was reported as 96 Scm^{-1} at 650°C and the thermal expansion coefficient (TEC) of material was 21.11 × 10^{-6} K^{-1}. However, the cell performance of the materials has not been investigated.

1.2.2 Literature reviews of chemical compatibility of cathode and electrolytes

To study the cell performance of SOFC, thermal expansion coefficient and the chemical compatibility between the cathode and the electrolyte are very important. Normally YSZ is the most popular electrolyte for SOFC because of high stability and high ionic conductivity. The chemical compatibility of the cathode with the YSZ electrolyte has been summarized as follow. Rim *et al* [8] reported the compatibility and electrical conductivity of $PrMnO_3$ substituted by 30%mol of Ca and Sr in A-site. The maximum electrical conductivity of 266 Scm^{-1} was achived when 30%mol of Ca was substituted. And, the compatibility of Ca-doped $PrMnO_3$ with YSZ at 1000 – 1200°C indicated no reaction occurs between the materials and YSZ. TU *et al* [9] investigated the chemical compatibility between $RE_{0.6}M_{0.4}Mn_{0.8}Co_{0.2}O_{3-\delta}$ (RE = La, Pr, Nd, Sm and Gd ; M =Sr and Ca) with YSZ electrolyte at 1200°C. The peroveskite doped with Sr at M position reacted with YSZ and produced $SrZrO_3$ phase while the compatibility of Ca doped did not release any peroveskite phases.

Kostogloudis *et al* [10] did not find a new phase from the compatibility study between $La_{1-x}Ca_xCo_{0.2}Fe_{0.8}O_{3-\delta}$ (x=0.15) with the YSZ but in other compositions of $La_{1-x}Ca_xCo_{0.2}Fe_{0.8}O_{3-\delta}$ and $La_{1-x}Sr_xCo_{0.2}Fe_{0.8}O_{3-\delta}$ new phases were formed. Kening *et al* [11] reported the performance of multi-layer (1 – *x*) $La_{0.8}Sr_{0.2}MnO_3$/*x* YSZ composite cathodes as electrode materials for SOFC. The thermal expansion coefficient and electrical conductivity decreased with the increasing the YSZ content. Xiqiang *et al* [12] investigated the composite cathode, $Pr_{1.6}Sr_{0.4}NiO_4$ + YSZ. The thermal expansion coefficient of $Pr_{1.6}Sr_{0.4}NiO_4$+YSZ was 11.37×10^{-6} K^{-1} while for $Pr_{1.6}Sr_{0.4}NiO_4$ was 14.15×10^{-6} K^{-1}. The thermal expansion coefficient of the composite cathodes with electrolyte YSZ was lower than the cathode $Pr_{1.6}Sr_{0.4}NiO_4$ so the composites may suitable for use in SOFC because of the TEC of YSZ used as the electrolyte, was measured to be 10.2×10^{-6} K^{-1}.

For the alternative materials [13], gadolinia-doped ceria (GDC) and samaria-doped ceria (SDC) are also used as electrolyte because of its high ionic conductivity at intermediate temperatures, the proper in thermal expansion coefficient with electrode, and the chemical stability with Co-containing cathodes. The chemical compatibilities of $Ba_{0.5}Sr_{0.5}Co_{0.8}Fe_{0.2}O_{3-\delta}$ with 8%mol yttria-stabilized zirconia (8YSZ) and 20%mol galdolinia-doped ceria (20GDC) were reported by Qingshan *et al*. [14] The results indicated no obvious phases detected when they were heated at 800°C for 5 hrs. Yongjun *et al* [15] developed the LSCF–GDC composite cathodes for solid oxide fuel cells by mixing the $La_{0.6}Sr_{0.4}Co_{0.2}Fe_{0.8}O_3$ (LSCF) powder with GDC. The electrochemical properties of porous LSCF cathodes and LSCF– GDC composite cathodes were evaluated at intermediate and low temperatures of 500–700°C. The polarization resistance of pure LSCF cathode sintered at 975 °C for 2 h was 1.20 ohm.cm^2 at 600°C while the lowest polarization resistance of LSCF–GDC (40:60 wt%) composite cathode was 0.17 ohm.cm^2. The cell performance generated the maximum power density of 562, 422, 257 and 139 mW/cm^2 at 650, 600, 550 and 500°C, respectively.

From the literature reviews, the BSCF perovskite is an interesting compound because its high ionic conductivity and the electrical conductivity can be developed by Ca^{2+} doping at A-site. In this work, $(Ba_{0.5}Sr_{0.5})_{0.7}Ca_{0.3}Co_{0.8}Fe_{0.2}O_{3-\delta}$ (BSCCF) was

chosen to study the chemical compatibility of the perovskite with YSZ electrolyte and GDC electrolyte for SOFC. From the reviews, YSZ electrolyte can react with the cathodes but some cathode materials doped with Ca did not produced any phases at low temperatures. Even though is not the best electrolyte material for SOFC, it is the most widely used due to its high performance in terms of oxygen ionic conductivity. The thermal expansion coefficient of the cathode formed composite with YSZ was decreased which beneficial for SOFC sintering cell. Thus, in this research we would like to focus on the compatibility between BSCCF and YSZ electrolyte for SOFC in the first. Then, the compatibility between BSCCF and GDC electrolyte was investigated respectively.

1.3 The objectives of the study

1. To find the optimal condition for BSCCF-YSZ composite and BSCCF-GDC composite, by varying ratio of material parameters e.g. 3:1, 1:1 and 1:3, sintering temperature (1000 -1300°C) and sintering time (6-12 hrs).

2. To study the electrical conductivity, the ionic conductivity and the thermal expansion coefficient of the composites.

3. To investigated the SOFC performance of the BSCCF cathode and the composites cathode in a single cell.

CHARPTER II
THEORY

2.1 Fuel cells [16]

The Fuel cell is an electrochemical device which converts the chemical energy to generate heat and electricity without combustion process involved that is the main cause of the greenhouse effect problem. A fuel cell consist of three main components which are an anode, an electrolyte and a cathode.

Fuel cells have many types which are classified by the type of electrolytes as summarized in Table 2-1. Nowadays, solid oxide fuel cells (SOFC) are of research interested because SOFC is suitable for high power generating station.

Table 2-1 Types of fuel cells

	PEFC	PAFC	AFC	MCFC	ITSOFC	SOFC
Electrolyte	proton exchange membrane	Mobilized liquid phosphoric acid	Potassium hydroxide	Mobilized liquid molten carbonate	ceramic	Ceramic
Operating Temperature (°C)	80°C	205°C	65-220°C	650°C	600-800°C	800 - 1000°C
Charge Carrier	H^+	H^+	OH^-	CO_3^{2-}	O^{2-}	O^{2-}
Catalyst	Platinum	Platinum	Platinum	Nickel	Perovskite	Perovskite

2.2 Solid oxide fuel cells (SOFCs)

The Solid oxide fuel cells (SOFCs) diverge from other fuel cells because SOFCs are convert the chemical fuel into the electricity at high temperature as 800 -

1000°C. SOFCs offer a non-pollution technology to produce electricity at high efficiency. SOFCs have a lot of advantages such as high efficiency, fuel flexibility, long life time, and too low toxic gas emission. In addition to the high operating temperature (600-1000°C) of SOFC, natural gas can reform within the cell itself eliminating the need for expensively external reformer system. SOFC can be combined with gas turbines for co-generated system to improve the efficiency. From the advantages, SOFC is the most suited for the power generations.

2.2.1 Operation of SOFCs

SOFC consists of two electrodes (one anode and one cathode) which sandwich around ceramic electrolyte. The schematic of the SOFC process is shown in Figure 2-1, hydrogen gas is fed into the anode as a fuel and oxygen gas is fed into the cathode as the oxidant. The oxygen ions were generated at the high temperature on the cathode side will be leading through the electrolyte to react with hydrogen gas at the anode. Electrons (e^-) are released and move toward the cathode via electrical connection between these electrodes resulting in useful electrical power. Then, electrons reduce the oxygen gas into oxide ions and diffuse to the anode again. In the SOFC system, water, CO_2 and heat are byproducts. The SOFC reactions are shown below:

Anode: $H_2 + O^{2-} \longrightarrow H_2O + 2e^-$ (2.1)

Cathode: $1/2O_2 + 2e^- \longrightarrow O^{2-}$ (2.2)

Cell: $H_2 + 1/2O_2 \longrightarrow H_2O$ or $CO + 1/2O_2 \longrightarrow CO_2$ (2.3)

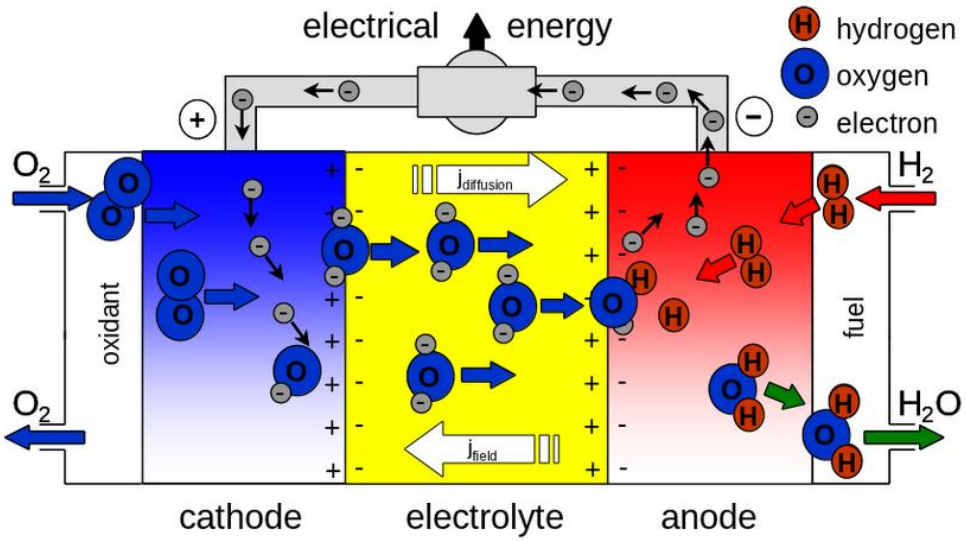

Figure 2-1 Schematic of the SOFC process [17]

2.2.2 Components of SOFCs [18]

2.2.2.1 Anode [19]

The anode is where oxidation reaction of H_2 and CO gases and the charge transfer from electrolyte take place. The electrons were produced from the oxidation will be conducted to the external circuit. Anode materials should be stable in the reducing environment of the fuels and electronically conducting. The requirements of the anode material are:

1. High electronic conductivity
2. The porous microstructure suitable for the fuel transportation.
3. Compatible Ni-YSZ is commonly used as anode materials because it can provide the high electrical conductivity and the efficiency in electrochemical reaction.
4. Low cost

2.2.2.2 Electrolyte [18]

Electrolyte materials are dense ceramics where exhibit purely ionic conductivity. They allow the oxide ions migrate from the cathode to the anode.

Therefore, they will expose both reducing atmosphere on the anode and oxidizing atmosphere on the cathode. The requirements of the electrolyte were:

1. High ionic conductivity
2. Low electronic conductivity
3. Physical and thermal expansion compatible with the anode and the cathode
4. Chemical stability in contact with electrodes.
5. Low coast materials

Metal oxides with cubic fluorite structures, i.e. yttria stabilized zirconia (YSZ) and gadoliniums doped ceria (GDC) have been widely studied as the electrolyte. However, Figure 2-2 ionic conductivity of GDC electrolyte is higher than YSZ electrolyte [20]. But, YSZ is the most favorable electrolyte due to availability and cost.

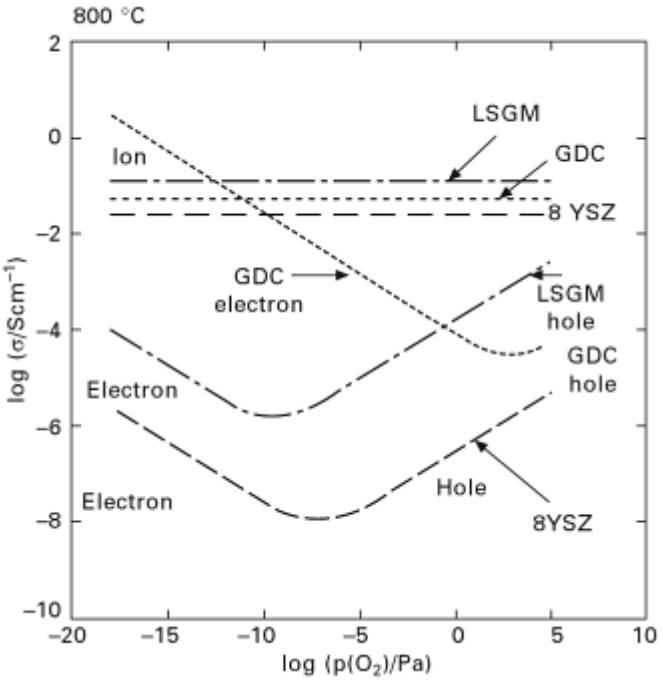

Figure 2-2 Ionic and electronic conductivities for some solid electrolytes

2.2.2.3 Cathode [21]

The cathode is where electrochemical reduction of O_2 to O^{2-} take place. Cathode materials have to meet the following requirements:

1. High electronic and ionic conductivity

2. Chemical stability in encountered environment during cell use.

3. Thermal expansion matching with the electrolyte

4. Non-reactivity with electrolytes

5. Sufficient porosity to provide more triple-phase boundaries (TPB) where the reaction takes place, and to facilitate transportation of molecular oxygen from the gas phase to the cathode/electrolyte interface.

These requirements were delighted by the perovskite oxide structure (ABO_3), where A is alkaline or alkaline earth metal, B is transition metal and O is oxygen. The perovskite are suitable as cathode materials because they have high ionic and electronic conductivity. For high temperature SOFC (working temperature is 800-1,000°C), lanthanum strontium manganite, $La_{1-x}Sr_xMnO_3$ (LSM) [8] is usually used because of their good conducting properties. Beside the metal oxide materials, a composite material between metal oxide cathode and electrolytes is an alternative choice of electrode because it improves electrode properties by increasing the TPBs. [22]

2.3 Perovskite [23]

2.3.1 Crystal structure of perovskite

Perovskites are inorganic compounds which have a simple formula of ABO_3, A is alkaline or alkaline earth metal, B is transition metal. The ideal perovskite has a cubic structure. A and O ions are forming a cubic close packed lattice. Then, the B ion occupies in octahedral holes created by O ions. The three dimensional structure of perovskite has a net of corner sharing [BO_6] octahedra with the A ion in 12-fold coordination between the polyhedra (Figure 2-3). The A ion is in position ½,½,½, the B ion in 0,0,0 and the O ion in ½,0,0; 0,½,0; 0,0,½. Perovskite oxide exhibits many properties, i.e. magnetic and electrical properties. It is flexible to accommodate several elements. Owing to the properties, the perovskite has good impact for industrial application, especially SOFC application.

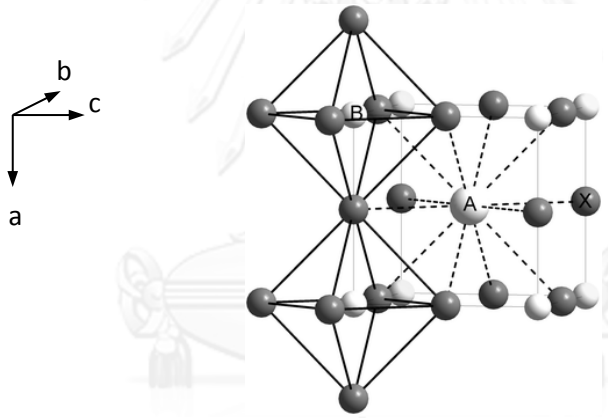

Figure **2-3** Perovskite structure

Figure 2-4 presents the ideal cubic perovskites the B-O distance equals to *a*/2, *a* is a cubic unit cell parameter, while the A-O distance equals to $a/\sqrt{2}$. The relationship between ionic radii and the unit cell parameter can be explained by the equations:

$$a = 2 \times B - O = 2 \times (r_B + r_O) \qquad (2.4)$$

$$a = \sqrt{2} \times (r_A + r_O) \qquad (2.5)$$

The ratio of two expressions for the *a* is called Goldschmidt's tolerance factor (*t*).

$$t = \frac{\sqrt{2}\times(r_A + r_O)}{2\times(r_B + r_O)} = \frac{(r_A + r_O)}{\sqrt{2}\times(r_B + r_O)} \qquad (2.6)$$

where r_A, r_B and r_O are the ionic radii of A, B and O ions, respectively.

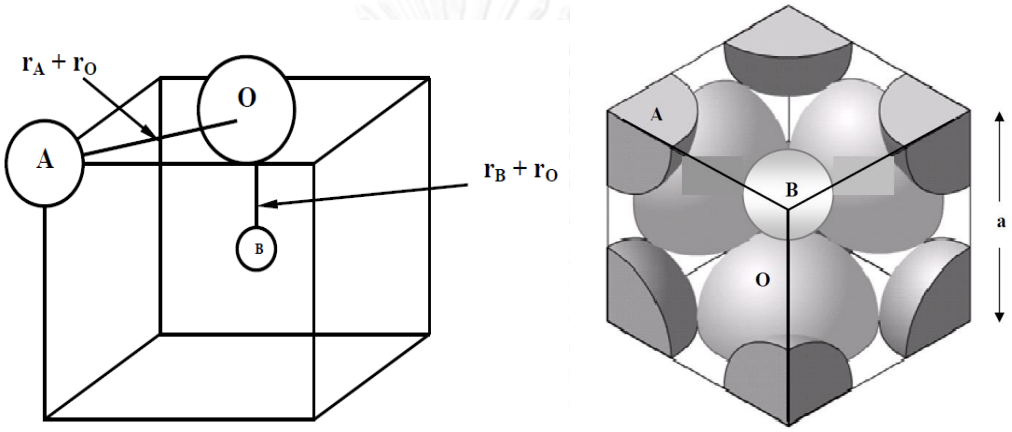

Figure 2-4 The relationship of ionic radii in a cubic unit cell

The degree of distortion from ideal cubic perovskite structure measures from Goldschmidt's tolerance factor. The ideal cubic perovskite should have t = 1. The t value is smaller than 1 when the A ion is smaller than the ideal value. On the other hand, the perovskite is hexagonal structure which is stable if the t value is higher than 1 due to a large A or a small B ion. The atomic layers are stacked in a hexagonal leading to face sharing of [BO_6] octahedral.

2.3.2 Properties of perovskites

Due to the variety of structures and chemical compositions, perovskites illustrate a lot of properties. The well-known properties of perovskites are mixed ionic and electronic conductivity (MIEC), oxygen permeation and magnetic property. From these properties, perovskites are chosen as components for SOFC.

2.3.2.1 Electronic conductivity (σ_e) [23]

Figure 2-5 shows the anionic *p* orbitals can spread towards the t_{2g} orbitals of B cations and both orbitals could overlap because of polarizability of anions. The *d* electrons of the t_{2g} orbital can delocalize to the t_{2g} orbital of adjacent B cations through the anionic *p* orbitals. The electronic conductivity in perovskite compounds concerns with charge carriers of excess electrons along the B–O–B chains. The higher amount of the mobile charge carriers is, the higher conductivity is. The charge carrier is typically generated by the substitution of trivalent cations with divalent cations at the A site. This case results in a decrease in total positive charge in the structure. As a result the imbalance charge is compensated either by the increase in valence of the B cation or the formation of oxygen vacancies. However, the relative proportion between two types of the charge compensation is unpredictable because it depends on some factors such as material-specific and temperature, pO_2. The electron holes are formed if the electronic compensation is predominant. Therefore, these holes act as hopping sites for electrons. Due to the electron hole, the electronic conductivity is call *p*-type conductivity. On the other hand, if the formation of oxygen vacancies is predominant, the reduction of B cations are generated from excess electrons. The electronic conductivity due to the excess electron is call *n*-type conductivity.

In addition to the doping of aliovalent cation on the A site, the mobile charge carriers can be generated by a charge-disproportionation effect as shown in reaction;

$$2B^{3+} \longrightarrow B^{2+} + B^{4+} \qquad (2.7)$$

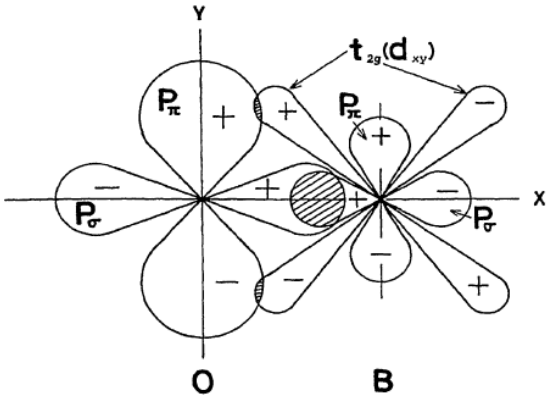

Figure 2-5 Covalent bonds between anionic *p* orbital and t_{2g} orbital of B cations.

The electronic conductivity of materials can be calculated from an electrical conductivity (σ). The electrical conductivity is the summation of electronic and ionic conductivity (σ_i), as follow:

$$\sigma = \sigma_e + \sigma_i \qquad (2.8)$$

The σ_i can be calculated from oxygen permeation flux. Either contribution may predominate depending on the material, its purity, and temperature.

2.3.2.2 Ionic conductivity (Oxide ion conductivity) (σ_i) [23, 24]

Oxygen vacancies are formed either by substitution of A cations and thermal reduction of B cations. These vacancies occur a good ionic conductivity because the oxide ion position exchange make the oxide ion diffuse with a vacancy along octahedral edge. The diffusion has to pass through a saddle point is shown in Figure 2-6.

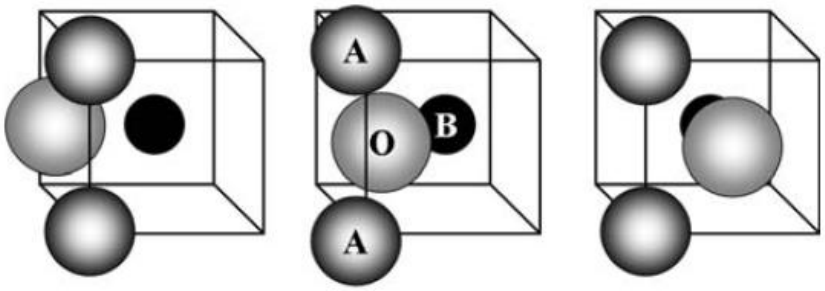

Pre-jump **Saddle-point** **Post-jump**

Figure 2-6 The migration of the oxygen ion pass through the saddle point.

The maximum ionic radius of mobile ions to pass through the saddle point is represented by critical radius (r_{cr}) calculated from equation;

$$r_{cr} = \frac{a_0(\frac{3}{4}a_0 - \sqrt{2}r_B) + r_B^2 - r_A^2}{2(r_A - r_B) + \sqrt{2}a_0} \qquad (2.9)$$

where r_A and r_B are the ionic radius of the A ion and B ion, respectively, and a_0 is the pseudo cubic lattice parameter.

2.3.2.3 Oxygen permeation [25]

There are two reasons of oxygen permeation on the perovskite membrane. First, molecular oxygen is dissociated at the cathode into oxide ions which permeates through the membrane and recombine as O_2 at the anode. Second, the oxygen permeation is motivated by a different oxygen partial pressure between rich and poor oxygen compartment as illustrated in Figure 2-7.

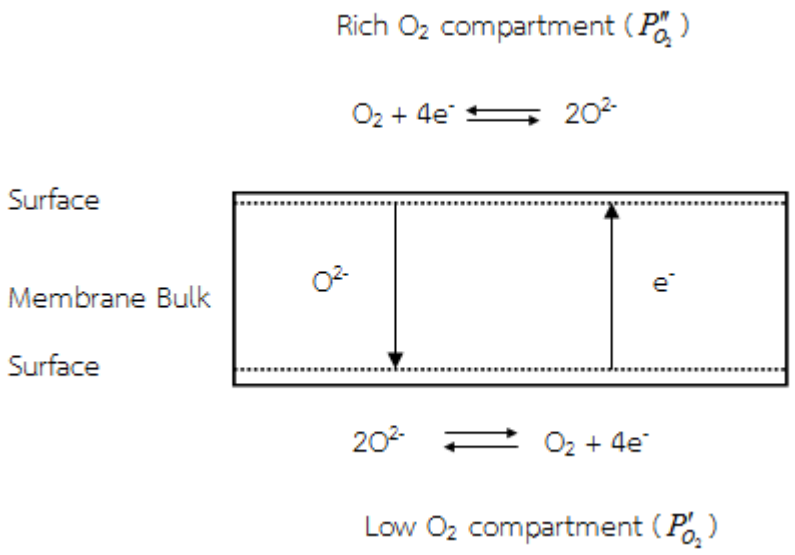

Figure 2-7 Oxygen transport during oxygen permeation

Mechanism for oxygen permeation through the perovskite membrane can be described as follows :

1. Mass transfer of oxygen gas from high oxygen partial pressure through the membrane surface.
2. The reaction between the molecular oxygen and oxygen vacancies at the membrane surface
3. Dissociation and electron transfer are giving the chemisorbed of oxygen ions
4. Incorporation in membrane surface layer
5. Diffusion of the bulk oxygen vacancy acress the membrane
6. The adsorbed O_2 is desorbed and transferred from the disc surface to the gas phase by low oxygen pressure.
7. Desorption from the surface
8. Mass transfer of oxygen from the membrane surface to low oxygen partial pressure.

2.4 Triple phase boundary [22]

A triple phase boundary (TPB) is a point of three dimensions where gas, electrode and electrolyte have reactions of oxygen adsorption, oxide ion diffusion, electronic and ionic conduction. Figure 2-8 shows a diagram of TPB at the cathode-electrolyte boundary in a solid-oxide fuel cell (SOFC). SOFC cathodes are designed to provide the multi-step oxygen reduction reaction as follow :

$$\tfrac{1}{2}O_2 \rightleftharpoons O \qquad (2.10)$$

$$O + 2e^- \rightleftharpoons O^{2-} \qquad (2.11)$$

$$O^{2-}(\text{cathode}) \rightleftharpoons O^{2-}(\text{electrolyte}) \qquad (2.12)$$

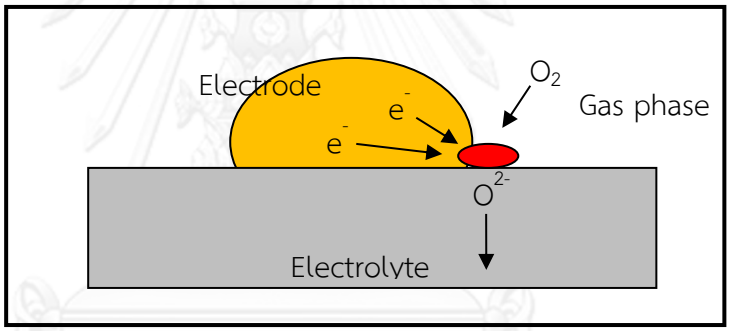

Figure 2-8 Triple-phase boundary pathway

Figure 2-9 presents the composite cathode had a larger triple phase boundary length, leading to a corresponding increase in the electrochemical performance.

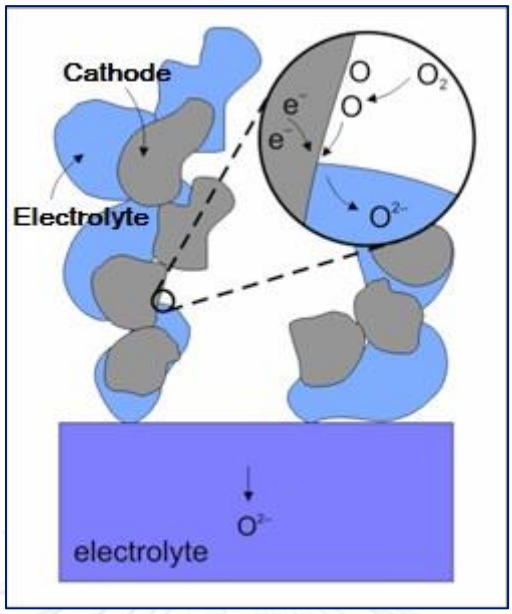

Figure 2-9 Pathway of the composite [26]

2.5 AC Impedance analysis [27]

The polarization resistance determined from AC measurement. The procedure of measuring impedance, Z as a function of frequency over a wide range from high frequency to low frequency, Z(ω). Impedance spectra is presented by the imaginary part of impedance, -Z on y-axis, and the real part of impedance, Z on x-axis. Then, Figure 2-10 illustrates an example of a typical impedance curve. The a) point shows the ohmic resistance of a component e.g. cathode while b) point shows the polarize resistance. Then, the point at the lowest frequency shows the total cell resistance.

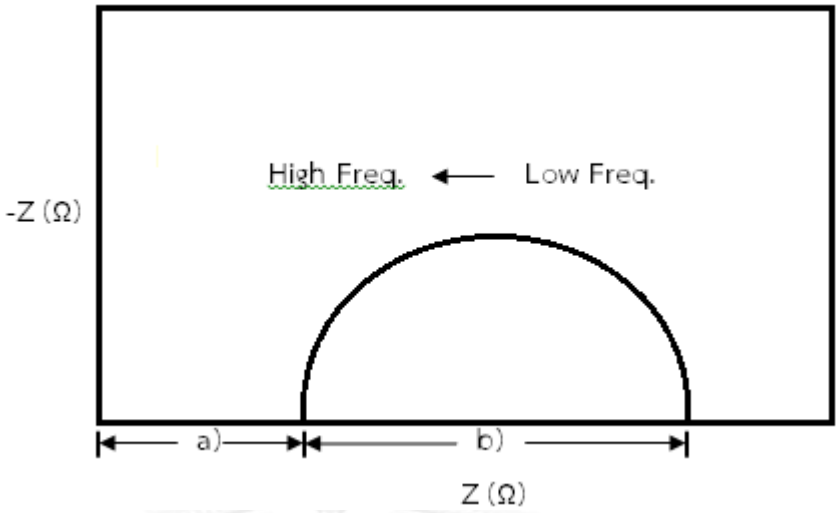

Figure 2-10 Impedance diagram

2.6 Performance of SOFC [28]

The fuel cell produces energy under short-circuited conditions with external load. In such a case the cell voltage is determined by polarization loss at the cathode and anode and ohmic loss, which are always linear dependent on the current. The losses are often called overvoltage (η_{act}) which originate primarily from an activation polarization (η_{ohm}), ohmic polarization (η_{conc}) and concentration polarization (η). The cell voltage, V, under loading conditions is given by equation

$$V = E - (\eta_{act} + \eta_{ohm} + \eta_{conc}) \qquad (2\text{-}13)$$

Where E is ideal voltage

The activation polarization is dominant at low current and it increases as current increases. Ohmic polarization varies with current and increases over the whole range of current due to a constant resistance of the cell. Concentration polarization occur over the entrie range of current density.

CHAPTER III

EXPERIMENT

3.1 Chemicals

Table 3-1 Chemicals and Reagent

Reagents	Formula Weight	Purity%	Company
$Ba(NO_3)_2$	261.35	99	Himedia
$Sr(NO_3)_2$	211.63	>99	Fluka
$Co(NO_3)_2{\cdot}6H_2O$	291.03	98-102.0	Ajax Finehem
$Fe(NO_3)_3{\cdot}9H_2O$	404.00	98-101.0	Fluka
$Ca(NO_3)_2{\cdot}4H_2O$	236.15	99.0	Ajax Finehem
$C_6H_8O_7$	192.13	>99.5	Univar
HNO_3	63.01	65	Merck
$NH_3{\cdot}H_2O$	35.00	25	Merck
C_2H_5OH	46.07	99.9	Merck
NiO	74.60	>99	Aldrich
$8\%Y_2O_3/ZrO_2$	304.13	>99.9	NaBond
C_3H_6O	58.07	>99.5	Merck
YSZ disc	-	-	Nikkato Ceramic
Ethyl cellulose	-	-	Aldrich

3.2 Synthesis of perovskite oxide powder

The perovskite $(Ba_{0.5}Sr_{0.5})_{0.7}Ca_{0.3}Co_{0.8}Fe_{0.2}O_{3-\delta}$ was synthesized by a modified citrate method. The precursor chemicals were $Ba(NO_3)_2$, $Sr(NO_3)_2$, $Ca(NO_3)_2$, $Co(NO_3)_2.6H_2O$ and $Fe(NO_3)_3.9H_2O$. The stoichiometric of metal nitrates were dissolved in HNO_3 solution (65% v/v) and stirred for 4 hrs at room temperature. Then, citric acid, a chelating agent, was added to nitrate solution with the mole ratio of citric acid to nitrate metal as 2:1. The mixture solution was stirred for 24 hrs at room temperature after that pH of the solution was adjusted to 9 with 25% ammonia

soution. The color of solution was changed from red to deep brown. [29] The homogeneous mixture solution was dried and combusted at 200 – 300°C on a hotplate until the solution became the grayish ash. The product was ground in a motar until a fine powder was obtained. The powder was calcined at 1000°C for 5 hrs in air with the increasing rate of 6.5°C/min to produce the perovskite oxide structure.

3.3 Chemical compatibility

The chemical reactivity between $(Ba_{0.5}Sr_{0.5})_{0.7}Ca_{0.3}Co_{0.8}Fe_{0.2}O_{3-\delta}$ cathode and electrolyte was studied by mixing cathode and electrolyte powders in weight ratio of 1:3, 1:1 and 3:1. The sample powder was ground for 15 mins, 3 times then, fired at 850 – 1,300°C for 7-10 hrs with the increasing rate of 6.5°C/min. Phase structure and impurities were determined by X-ray powder diffractometer.

3.4 Sample disc preparation

3.4.1 The $(Ba_{0.5}Sr_{0.5})_{0.7}Ca_{0.3}Co_{0.8}Fe_{0.2}O_{3-\delta}$ disc preparation

After calcination, $(Ba_{0.5}Sr_{0.5})_{0.7}Ca_{0.3}Co_{0.8}Fe_{0.2}O_{3-\delta}$ powder was milled with ethanol in a mortar. Then, a 1.8 gram of fine powder was pressed into a pellet under pressure of 2 tons for 10 mins to obtain the perovskite disc. The sample disc was sintered at 1,100°C for 10 hrs with the increasing rate of 6.5°C/min.

3.4.2 The composite disc preparation

The composite powder was prepared from the perovskite oxide powder and the electrolyte powder similar to the chemical compatibility study. A 1.8 gram of the mixed powder was pressed into a pellet as the $(Ba_{0.5}Sr_{0.5})_{0.7}Ca_{0.3}Co_{0.8}Fe_{0.2}O_{3-\delta}$ disc preparation in 3.4.1. Then, the disc was fired at the condition resulted from chemical compatibility study.

3.5 Cell Preparation

3.5.1 Single cell

The NiO-YSZ (YSZ = Yttrium Stabilized Zirconia) powder in weight ratio of 60:40 was mixed with the STD-100 binder and pasted onto the commercial 8YSZ disc (ø 15mm, thickness 0.5mm) by tape casting method. Then, the NiO-YSZ anode was fired at 1300°C for 4 hrs. For the cathode side, the $(Ba_{0.5}Sr_{0.5})_{0.7}Ca_{0.3}Co_{0.8}Fe_{0.2}O_{3-\delta}$ powder and the composite powders were also mixed with the binder. After that, the slurry was pasted onto the other side of YSZ disc and fired at the temperature and the time derived from the chemical compatibility study. Pt mesh and Pt wire were attached on the surface of the electrodes as illustrated in Figure 3-1 The cell was heated at 850°C for 1 h in air.

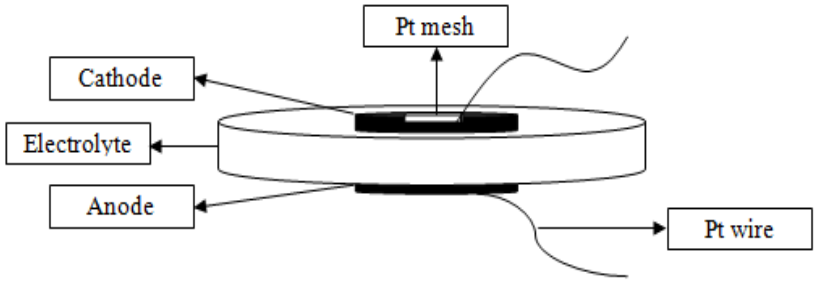

Figure 3-1 Illustration of fabricated single cell

3.5.2 Symmetric cell

Slurry of $(Ba_{0.5}Sr_{0.5})_{0.7}Ca_{0.3}Co_{0.8}Fe_{0.2}O_{3-\delta}$ powder and the composite powders were pasted on both sides of the electrolyte disc by tape casting. Then, the sample disc was fired at the same condition for a cathode side in the single cell fabrication. After that, Pt mesh and Pt were pressed onto the both side similar to the single cell preparation.

3.6 Characterization

3.6.1 X-ray powder diffractometer (Rigaku, Dmax 2200/Ultima^{+})

The XRD was equipped with a monochromator and the Cu Kα radiation source (40 kV, 30 mA). The diffraction pattern was recorded from 20 to 70 degree of the 2-theta range.

3.6.2 Electron Probe Micro Analyzer (EPMA)

The morphology of single cells were observed by the electron microprobe analyzer (Shimidazu EPMA-1600). The beam current and accelerate voltage for measuring was 0.2 nA and 15kV. Gold was used to sputter onto the surface of the samples.

3.6.3 SEM

The morphology of the sintered discs, $(Ba_{0.5}Sr_{0.5})_{0.7}Ca_{0.3}Co_{0.8}Fe_{0.2}O_{3-\delta}$, were characterized by a JEOL JSM-5800LV scanning electron microscopy and energy dispersive x-ray spectrometry (EDX), Oxford Instrument (Link ISIS series 300) at the Scientific and Technological Research Equipment Center (STREC), Chulalongkorn University.

3.6.4 Density by Archimedes method

The Cathode and composite discs were boiled in water for 5 hours. The samples were determined their densities by the Archimedes method [30]. The sample disc was weighed in dry and wet condition and considered for the density.

3.7 Properties Measurement

3.7.1 Electrical conductivity measurement

The electrical conductivity was measured by a DC 4-probe method. The sample discs were cut into a rectangular shape (5 mm x 12 mm x 1.5 mm) and wrapped with Pt wire electrodes on four sides, as shown in Figure 3-2.

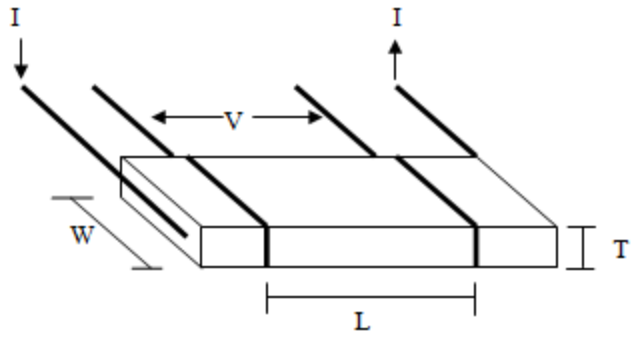

Figure 3-2 Illustration of conductivity preparation

Then, a current (I) was applied to the outer wires and the voltage between the inner wires at distance L was collected as a function of temperatures from 300°C to 850°C with a heating rate of 3.33°C/min.

The data was calculated for the electrical conductivity using the equation 3.1

$$S = (I/V)*(L/(W*T)) \quad \text{..... (3.1)}$$

S = electrical conductivity

I = input current (A)

V = resulting potential (V)

L = length between Pt (cm)

T = thickness of membrane (cm)

W = width of membrane (cm)

3.7.2 Oxygen permeation measurement

The sample discs were measured for the oxygen permeation on the membrane reactor. The sample discs with the thickness of 0.7 mm were prepared and placed in the reactor (Figure 3-3). Helium (99.999%) and oxygen (99.98%) gas were purged into the membrane reactor with the flow rate of 50 mL/min on the

bottom and the top of the sample disc, respectively. The oxygen gas which permeated throughout the sample disc was compiled by a gas tight syringe and analyzed by a gas chromatography (VARIAN, CP-3800) provided with Molecular sieve 13X column.

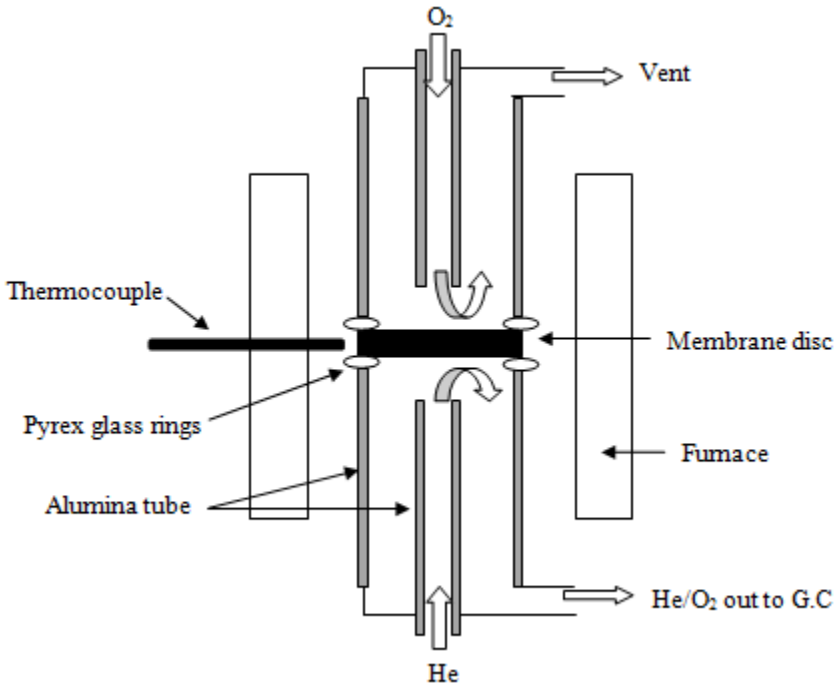

Figure 3-3 The diagram of the reactor membrane for oxygen permeation measurement.
(The picture was modified from Ratchaoun, C.[31])

3.7.3 Impedance Analysis for the symmetrical electrode cell

The symmetrical electrode cell from section 3.5 was placed on the alumina tubes inside the furnace as shown in Figure 3-4. After the cell was set up in the furnace, the temperature was increased to 850°C. Then, the impedance of the cell was measured in air by Frequency Response Analysis (FRA). The data was collected at : 850°C, 800°C, 750°C, 700°C and 650°C.

3.7.4 Single Cell Performance

The single cell was placed into the reactor between two alumina tubes attached with two pyrex glass rings as shown in Figure 3-4. After the cell was set up,

the temperature was increased to 870°C and left for 30 mins to melt the glass ring for tube sealing. Then, the temperature was decreased to 850°C and hold for 30 mins to allow the melted glass rings to solidify and confirm sealing As the temperature reached 850°C, Argon gas (Ar, 99.995%) with flow rate of 20ml/min was fed at the anode while oxygen gas with the same flow rate was fed at the cathode. After 1 h, Ar gas was changed into hydrogen gas at flow rate of 20ml/min for anode reduction. Then, the impedance measurement and the I-V measurement was performed at the same temperature with symmetrical cell measurement.

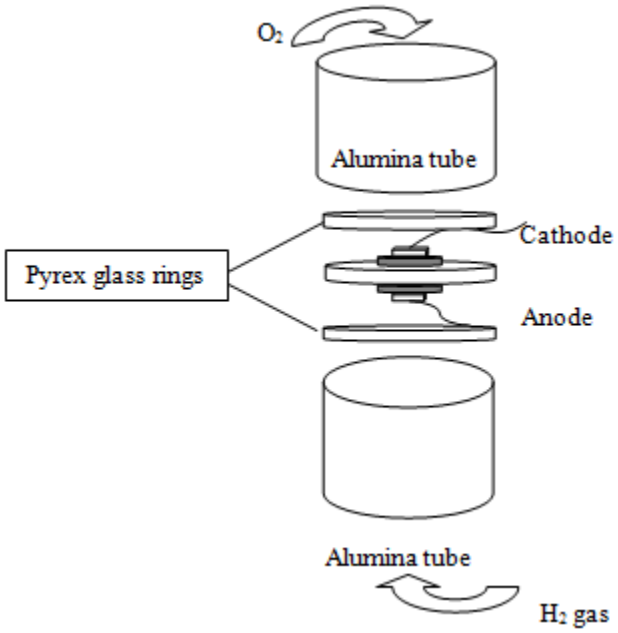

Figure 3-4 The position of cell testing between the alumina tubes inside the furnace

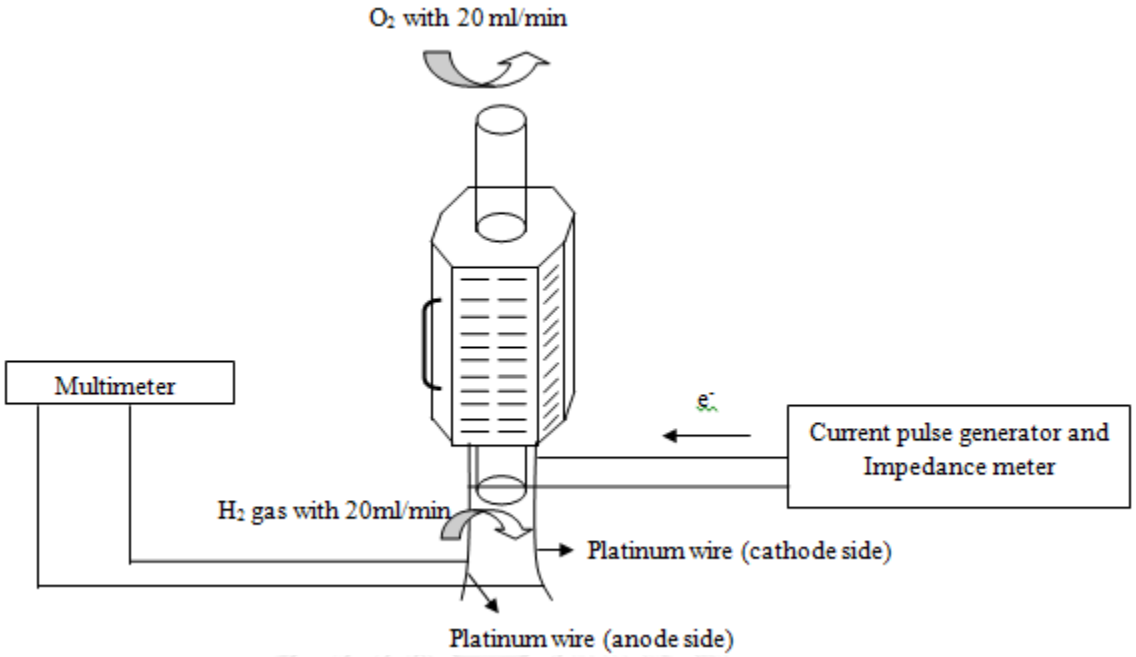

Figure 3-5 Diagram of furnace set-up for cell performance test

(The picture was modified from Ruengwranit, C.[32])

CHAPTER IV
RESULTS AND DISCUSSION

4.1 Chemical compatibility

4.1.1 Composite of $(Ba_{0.5}Sr_{0.5})_{0.7}Ca_{0.3}Co_{0.8}Fe_{0.2}O_{3-\delta}$ with YSZ

$(Ba_{0.5}Sr_{0.5})_{0.7}Ca_{0.3}Co_{0.8}Fe_{0.2}O_{3-\delta}$ cathode and YSZ electrolyte powder were mixed in weight ratio of 1:3, 1:1 and 3:1. Then, the samples were fired at 850 – 1,300°C for 7-10 hrs. Figure 4-1 presents phase structures and impurities of composite powder in weight ratio of 1:3 after calcination at various temperatures for 10 hrs. The XRD patterns show the YSZ structure while the perovskite structure disappears. However, $Sr(ZrO_3)$ (PDF no. 44-0161) structure has been found owing to $(Ba_{0.5}Sr_{0.5})_{0.7}Ca_{0.3}Co_{0.8}Fe_{0.2}O_{3-\delta}$ reacts with YSZ electrolyte. Similar to the 1:3 composite, the composite in weight ratio of 1:1 and 3:1 were fired at the same condition. Then, the XRD patterns are shown in Figure 4-2 and Figure 4-3 respectively. It has been found that the 3:1 composite was melted at 1200 – 1300°C because the composite structure is not stable therefore the XRD patterns can only be observed at 850 – 1100°C. Alike to the 1:3 composite, the XRD patterns of composites powder in weight ratio of 1:1 also show the structures of YSZ, $Sr(ZrO_3)$ and $CaZrO_3$ (PDF no. 35-0790) indicating YSZ electrolyte is partially reacted with $(Ba_{0.5}Sr_{0.5})_{0.7}Ca_{0.3}Co_{0.8}Fe_{0.2}O_{3-\delta}$. $Sr(ZrO_3)$ and $CaZrO_3$ were formed by the migration of strontium and calcium from perovskite structure to react with ZrO_2 in YSZ electrolyte [33]. In Figure 4-3, $Sr(ZrO_3)$ phase was observed due to the reaction between strontium and YSZ electrolyte similar to the reaction of the 1:1 composite. In the same way of the reaction, strontium and cobalt leave off the peroveskite structure to form $SrCoO_3$ (PDF no. 39-1084) phase. Therefore, the effect of firing time was investigated by decreasing time to 9 and 7 hrs. The data were summarized in Table 4-1, and the XRD patterns were displayed in Appendix A.

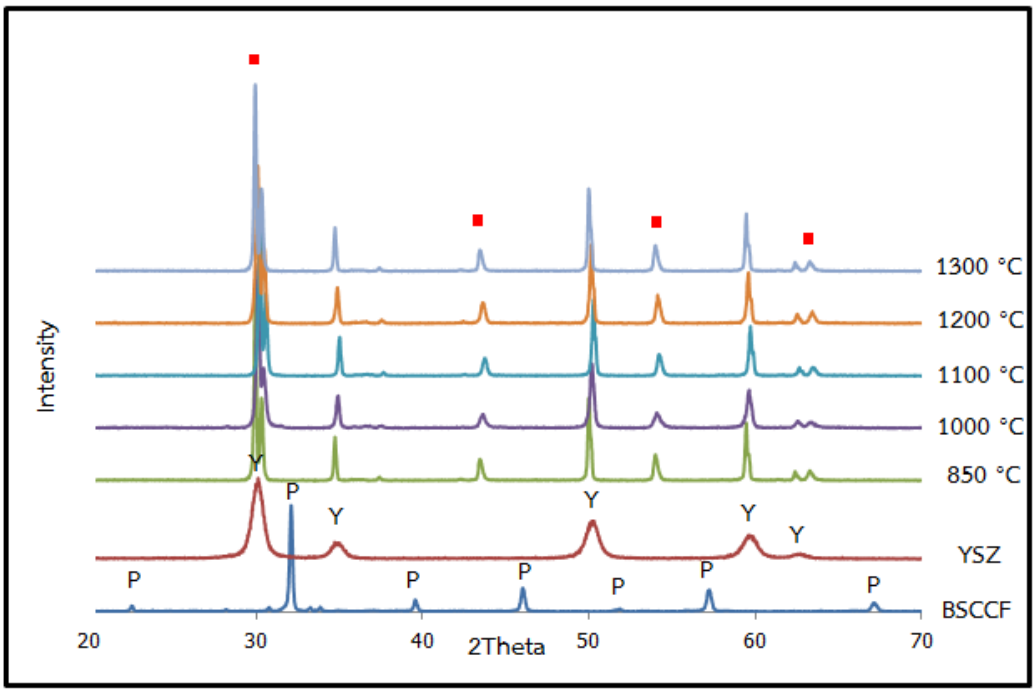

Figure 4-1 XRD patterns of $(Ba_{0.5}Sr_{0.5})_{0.7}Ca_{0.3}Co_{0.8}Fe_{0.2}O_{3-\delta}$-YSZ composite in weight ratio of 1:3 (BSCCF:YSZ) was calcined at
1000 – 1300°C for 10hrs, (BSCCF (P), YSZ (Y), $Sr(ZrO_3)$ (■))

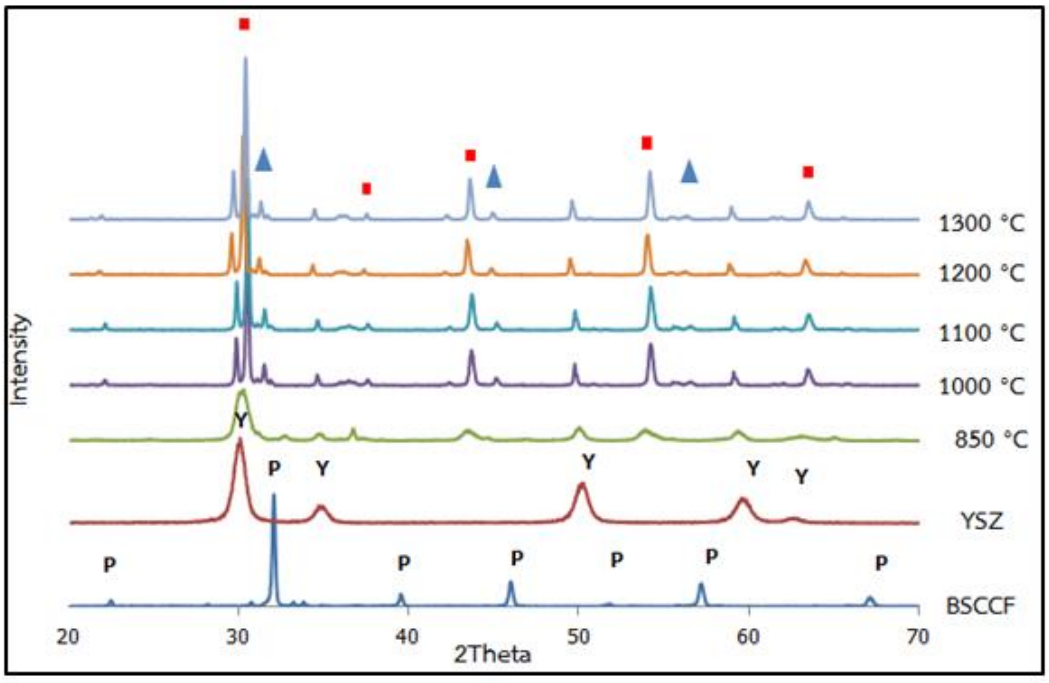

Figure 4-2 XRD patterns of $(Ba_{0.5}Sr_{0.5})_{0.7}Ca_{0.3}Co_{0.8}Fe_{0.2}O_{3-\delta}$-YSZ composite in weight ratio of 1:1 (BSCCF:YSZ) was calcined at 850 – 1300°C for 10hrs.
(BSCCF (P), YSZ(Y), $Sr(ZrO_3)$(■), $CaZrO_3$(▲))

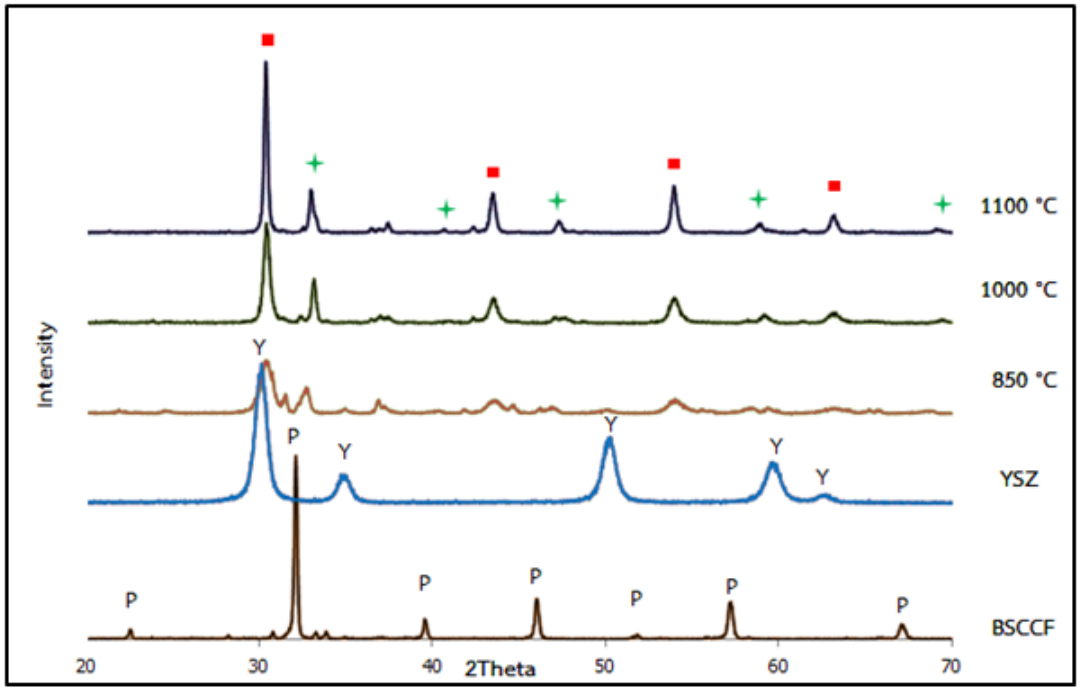

Figure 4-3 XRD patterns of $(Ba_{0.5}Sr_{0.5})_{0.7}Ca_{0.3}Co_{0.8}Fe_{0.2}O_{3-\delta}$-YSZ composite in weight ratio of 3:1 (BSCCF:YSZ) was calcined at 850 – 1100°C for 10hrs.
(BSCCF (P), YSZ(Y), $Sr(ZrO_3)$(■), $SrCoO_3$(✦)

Table 4-1 Phase obtained from reaction between $(Ba_{0.5}Sr_{0.5})_{0.7}Ca_{0.3}Co_{0.8}Fe_{0.2}O_{3-\delta}$ and YSZ at various temperatures.

Ratio	Times (hrs)	Temperature (°C)				
		850°C	1000°C	1100°C	1200°C	1300°C
1:3	7	$Sr(ZrO_3)$	$Sr(ZrO_3)$	$Sr(ZrO_3)$	$Sr(ZrO_3)$	$Sr(ZrO_3)$
(BSCCF:YSZ)	9	$Sr(ZrO_3)$	$Sr(ZrO_3)$	$Sr(ZrO_3)$	$Sr(ZrO_3)$	$Sr(ZrO_3)$
	10	$Sr(ZrO_3)$	$Sr(ZrO_3)$	$Sr(ZrO_3)$	$Sr(ZrO_3)$	$Sr(ZrO_3)$
1:1	7	$Sr(ZrO_3)$	$Sr(ZrO_3)$	$Sr(ZrO_3)$	$Sr(ZrO_3)$	$Sr(ZrO_3)$
(BSCCF:YSZ)		$CaZrO_3$	$CaZrO_3$	$CaZrO_3$	$CaZrO_3$	$CaZrO_3$
	9	$Sr(ZrO_3)$	$Sr(ZrO_3)$	$Sr(ZrO_3)$	$Sr(ZrO_3)$	$Sr(ZrO_3)$
		$CaZrO_3$	$CaZrO_3$	$CaZrO_3$	$CaZrO_3$	$CaZrO_3$
	10	$Sr(ZrO_3)$	$Sr(ZrO_3)$	$Sr(ZrO_3)$	$Sr(ZrO_3)$	$Sr(ZrO_3)$
		$CaZrO_3$	$CaZrO_3$	$CaZrO_3$	$CaZrO_3$	$CaZrO_3$
3:1	7	$Sr(ZrO_3)$	$Sr(ZrO_3)$	$Sr(ZrO_3)$	_	_
(BSCCF:YSZ)		$SrCoO_3$	$SrCoO_3$	$SrCoO_3$		
	9	$Sr(ZrO_3)$	$Sr(ZrO_3)$	$Sr(ZrO_3)$	_	_
		$SrCoO_3$	$SrCoO_3$	$SrCoO_3$		
	10	$Sr(ZrO_3)$	$Sr(ZrO_3)$	$Sr(ZrO_3)$	_	_
		$SrCoO_3$	$SrCoO_3$	$SrCoO_3$		

From Table 4-1, even though the reaction time was decreased, $Sr(ZrO_3)$, $SrCoO_3$ and $CaZrO_3$ were also found similar to the composites fired at 10 hrs. It is concluded that perovskite reacts with YSZ electrolyte.

4.1.2 Composite of $(Ba_{0.5}Sr_{0.5})_{0.7}Ca_{0.3}Co_{0.8}Fe_{0.2}O_{3-\delta}$ with GDC

$(Ba_{0.5}Sr_{0.5})_{0.7}Ca_{0.3}Co_{0.8}Fe_{0.2}O_{3-\delta}$ cathode and GDC electrolyte powder were mixed in weight ratio like the composite of $(Ba_{0.5}Sr_{0.5})_{0.7}Ca_{0.3}Co_{0.8}Fe_{0.2}O_{3-\delta}$ and YSZ. Then, the sample was fired at 850 – 900°C for 7-10 hrs for studing the compatibity of the composites.

Figure 4-4 shows phase structure of the (BSCCF : GDC) composites in weight ratio of 1:3, 1:1 and 3:1 after fired at 850°C for 10 hrs. The XRD patterns show BSCCF and GDC structures only, indicating no reaction occurs between BSCCF and GDC at 850°C. Afterwards, composites were fired at 900°C and the unwanted phases were found at this temperature. The reaction products are presented in Table 4-2.

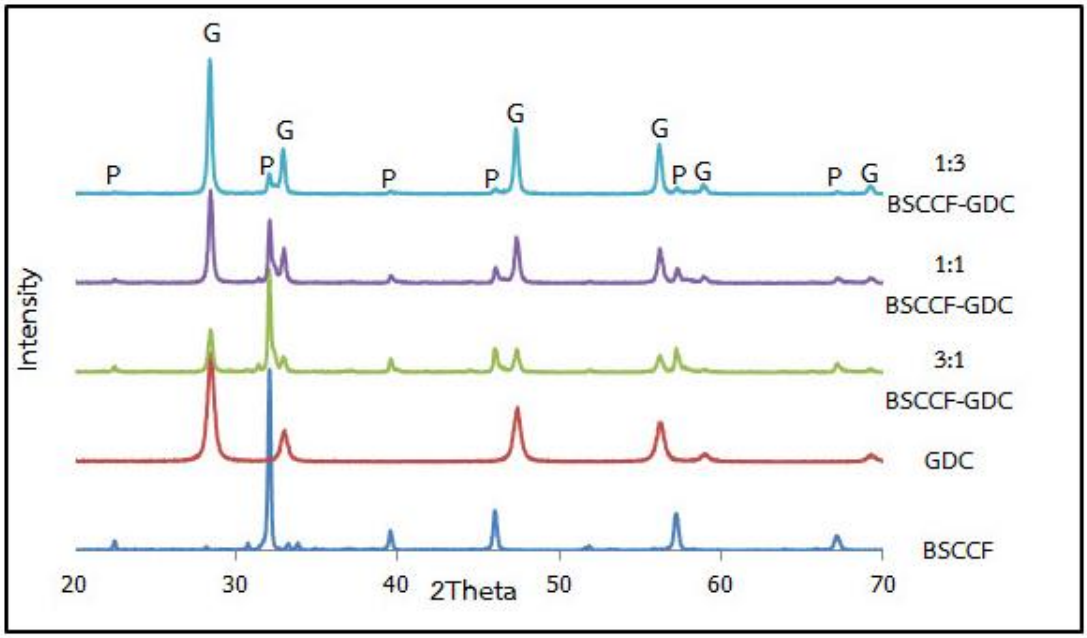

Figure 4-4 XRD patterns of mixed powder of BSCCF and GDC in weight ratio of 1:3, 1:1 and 3:1 (BSCCF:GDC) was calcined at 850°C for 10 hrs. (BSCCF (P), GDC (G)

Table 4-2 Phases obtained from reaction between $(Ba_{0.5}Sr_{0.5})_{0.7}Ca_{0.3}Co_{0.8}Fe_{0.2}O_{3-\delta}$ and GDC at various temperatures.

Ratio	Times (hrs)	Temperature (°C)	
		850°C	900°C
1:3 (BSCCF:GDC)	7	None	$SrCoO_3$
	9	None	$SrCoO_3$
	10	None	$SrCoO_3$
1:1 (BSCCF:GDC)	7	None	$SrFeO_3$
	9	None	$SrFeO_3$
	10	None	$SrFeO_3$
3:1 (BSCCF:GDC)	7	None	$SrFeO_3$
	9	None	$SrFeO_3$
	10	None	$SrFeO_3$

$SrCoO_3$ and $SrFeO_3$ (PDF no. = 40-0906) were released when the composites were fired at 900°C. The reactive phases also indicate the stability of the cathode structure [34]. Strontium, cobalt and iron were migrated from the perovskite structure resemble the metal migration between the composite and GDC electrolyte. According to the results, the BSCCF:GDC composite structure will be stable until 850°C, therefore further investigation will be conducted at temperature lower than 850°C

From the compatibility between BSCCF and electrolyte, GDC electrolyte has stability better than YSZ because Ce^{4+} ion is larger than Zr^{4+}. Thus, divalent ions from A-site can form the perovskite structure with YSZ easier than GDC. BSCCF does not react with GDC electrolyte [35]. Thus, GDC electrolyte can be used as the interlayer between BSCCF and YSZ electrolyte disc because GDC did not react with BSCCF and YSZ at 850˚C. The XRD patterns showed in Figure 4-5 indicate GDC does not react with YSZ at 1,200˚C.

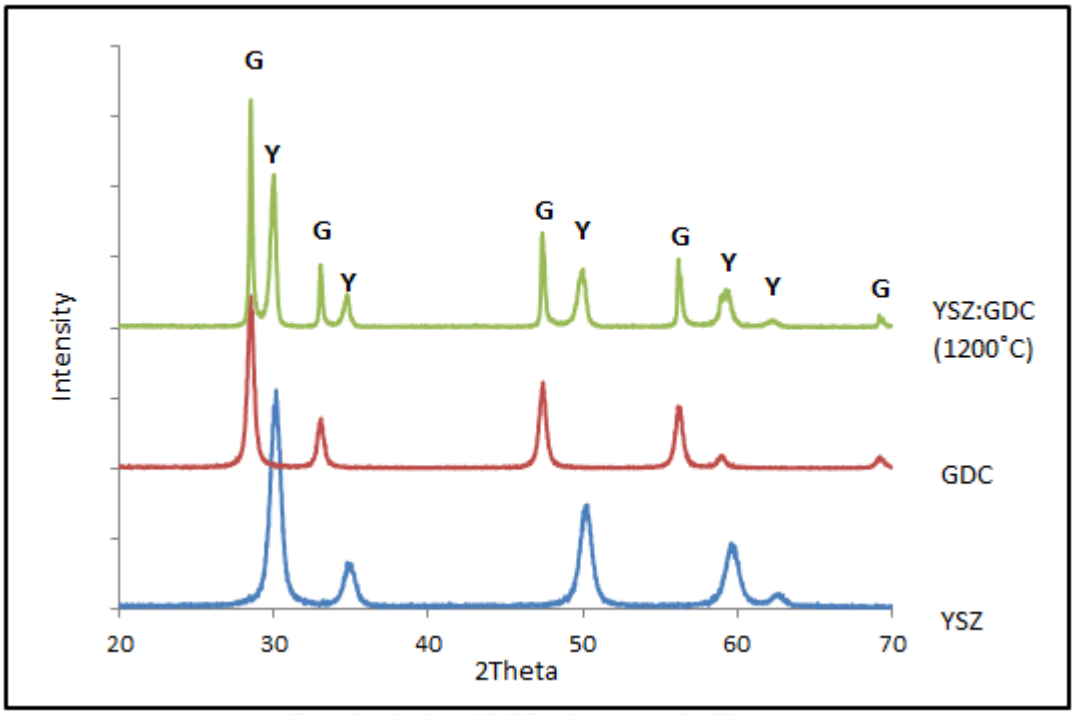

Figure 4-5 XRD patterns of mixed powder of YSZ and GDC in weight ratio of 1:1 (YSZ:GDC) fired at 1200°C for 10 hrs. (YSZ (Y), GDC (G)

4.2 Electrical Conductivity

4.2.1 $(Ba_{0.5}Sr_{0.5})_{0.7}Ca_{0.3}Co_{0.8}Fe_{0.2}O_{3-\delta}$ and composites with YSZ

$(Ba_{0.5}Sr_{0.5})_{0.7}Ca_{0.3}Co_{0.8}Fe_{0.2}O_{3-\delta}$ and all BSCCF:YSZ composites from 4.1 were studied for the electrical conductivities at 400 - 850°C. However, the electrical conductivities of $(Ba_{0.5}Sr_{0.5})_{0.7}Ca_{0.3}Co_{0.8}Fe_{0.2}O_{3-\delta}$ and the composite in 3:1 weight ratio fired at 1100°C for 7 – 10 hrs and at 1000°C for 10 hrs could only be measured. The data were summarized in Figure 4-6 and Table 4-3. From Figure 4-6, the electrical conductivities of $(Ba_{0.5}Sr_{0.5})_{0.7}Ca_{0.3}Co_{0.8}Fe_{0.2}O_{3-\delta}$ increased when the temperatures were increased from 400°C to 550°C, suggesting a semiconductor behavior. When the material obtains higher energy, thermal energy may lead a free electron, a hole as an empty spot with a positive charge will occur. The free electron can move through the hole leading a higher conductivity at 550°C. Although elcetrons had a good

transfer when temperatures were increased, the electrical conductivity was decreased from 550°C to 850°C, which is a behavior of a metallic conduction. When eletrons obtain the high thermal energy, electrons move in out of order to another metal atoms so the electrical conductivity is decreased. For composites in Figure 4-7, the conductivity increased with temperature indicating semiconducting like behavior. However, the composites had lower electrical conductivities than the $(Ba_{0.5}Sr_{0.5})_{0.7}Ca_{0.3}Co_{0.8}Fe_{0.2}O_{3-\delta}$. This may be due to the consisting of $CaZrO_3$, $SrCoO_3$ and YSZ electrolyte in composite which have a low conductivity; 4.64 x 10^{-7}, 6.7 and 0.10 $S.cm^{-1}$ respectively [36-38]. The specific conductivity of materials at 400 – 850°C were summarized in Table 4-3.

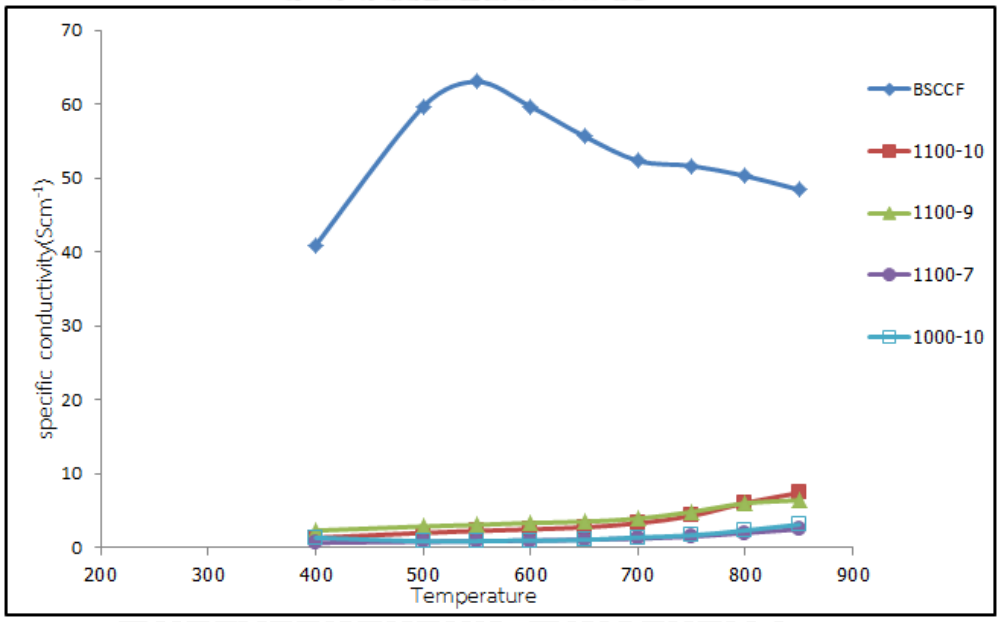

Figure 4-6 Temperature dependence of the specific conductivity (σ) of $(Ba_{0.5}Sr_{0.5})_{0.7}Ca_{0.3}Co_{0.8}Fe_{0.2}O_{3-\delta}$ and composites BSCCF:YSZ (3:1)

BSCCF : $(Ba_{0.5}Sr_{0.5})_{0.7}Ca_{0.3}Co_{0.8}Fe_{0.2}O_{3-\delta}$
1100-10 : composite fired at 1100°C for 10 hrs
1100-9 : composite fired at 1100°C for 9 hrs
1100-7 : composite fired at 1100°C for 7 hrs
1000-10 : composite fired at 1000°C for 10 hrs

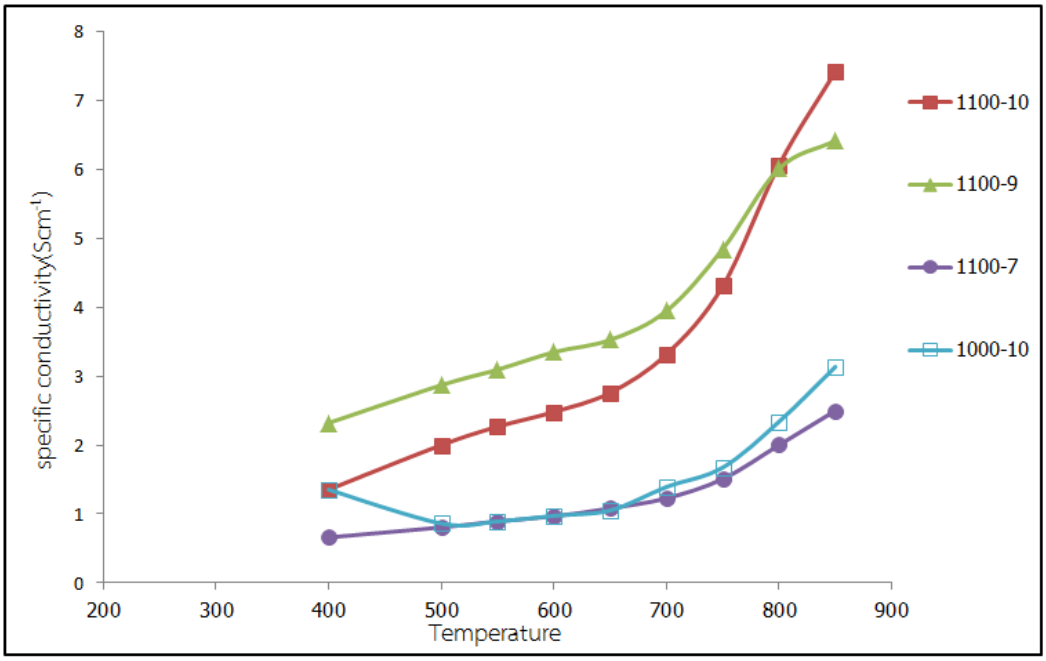

Figure 4-7 Temperature dependence of the specific conductivity (σ) of $(Ba_{0.5}Sr_{0.5})_{0.7}Ca_{0.3}Co_{0.8}Fe_{0.2}O_{3-\delta}$ and composites

1100-10 : composite fired at 1100 °C for 10 hrs

1100-9 : composite fired at 1100 °C for 9 hrs

1100-7 : composite fired at 1100 °C for 7 hrs

1000-10 : composite fired at 1000 °C for 10 hrs

Table 4-3 Specific conductivity (σ) of $(Ba_{0.5}Sr_{0.5})_{0.7}Ca_{0.3}Co_{0.8}Fe_{0.2}O_{3-\delta}$ and composites

Sample	Specific conductivity (Scm^{-1})									σ_{max}
	400°C	500°C	550°C	600°C	650°C	700°C	750°C	800°C	850°C	(T_{max})
BSCCF	40.96	59.72	63.07	59.71	55.70	52.37	51.67	50.33	48.45	63.07 (550)
1100-10	1.35	2.00	2.27	2.48	2.76	3.31	4.31	6.06	7.42	7.42 (850)
1100-9	2.32	2.87	3.09	3.35	3.53	3.94	4.84	6.01	6.41	6.41 (850)
1100-7	0.66	0.81	0.89	0.97	1.08	1.23	1.51	2.00	2.50	2.50 (850)
1000-10	1.35	0.86	0.89	0.97	1.05	1.39	1.67	2.34	3.13	3.13 (850)

4.2.2 $(Ba_{0.5}Sr_{0.5})_{0.7}Ca_{0.3}Co_{0.8}Fe_{0.2}O_{3-\delta}$ and composites with GDC

For the composite of $(Ba_{0.5}Sr_{0.5})_{0.7}Ca_{0.3}Co_{0.8}Fe_{0.2}O_{3-\delta}$ and GDC electrolyte, only the composites fired at 850°C were chosen for the electrical measurement because they did not have the reactivity between $(Ba_{0.5}Sr_{0.5})_{0.7}Ca_{0.3}Co_{0.8}Fe_{0.2}O_{3-\delta}$ and GDC at this temperature. However, the data cannot be obtained because the low density of the composites (Table 4-4) similar to the work report by Pascual [39]. On the other hand, the GDC electrolyte has also very low conductivity [40] which may influence the conductivity of composites.

Table 4-4 Densities of BSCCF : GDC composites fried at 850°C

Ratio	Timing(hrs)	Density(g/cm^3)
1:3	7	3.21
(BSCCF:GDC)	9	3.24
	10	3.27
1:1	7	3.60
(BSCCF:GDC)	9	3.66
	10	3.71
3:1	7	3.87
(BSCCF:GDC)	9	3.91
	10	3.94

From the specific conductivities, BSCCF and BSCCF:YSZ (3:1) fired at 1100°C for 9 and 10 hrs were collected to study the oxygen permeation because they have higher specific conductivities than others.

4.3 Oxygen permeation

The oxygen permeation was investigated from the high temperatuer to low temperature by decreasing temperature every 50°C. The results were shown in Figure 4-8.

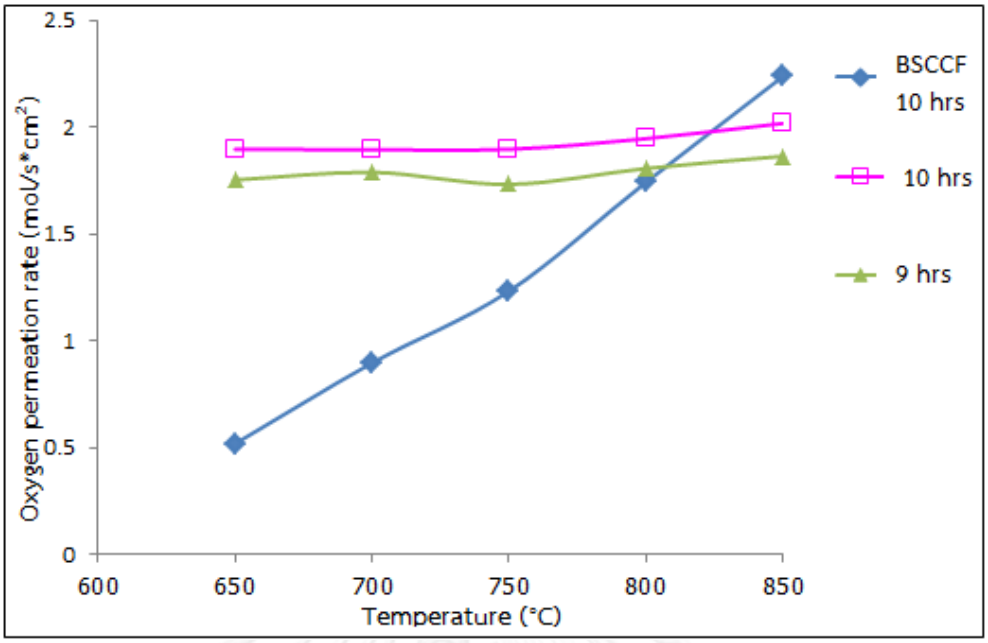

Figure 4-8 Temperature dependence of oxygen permeation rate for $(Ba_{0.5}Sr_{0.5})_{0.7}Ca_{0.3}Co_{0.8}Fe_{0.2}O_{3-\delta}$ and the composite BSCCF-YSZ (3:1) fired at 1100°C

From Figure 4-8, $(Ba_{0.5}Sr_{0.5})_{0.7}Ca_{0.3}Co_{0.8}Fe_{0.2}O_{3-\delta}$ has the highest oxygen permeation rate at 850°C. At high temperature, the material has obtained a high thermal energy. Then, the structure vibrates more than that at low temperature then the oxide ion will be left from the structure. The oxygen vacancies are increased by the departing of oxide ion. After that, oxide ions from the structure and oxygen gas will be migrate through the oxygen vacancies of the material membrane. On the other hand, the oxygen permeation rate decreased when the temperature was going down. For the composites, the oxygen permeation rates of the composites fired for 10 hrs were higher than one fired for 9 hrs. The oxygen permeation rates of the composites slightly decreased when the temperatures were going down like as the oxygen permeation rate of $(Ba_{0.5}Sr_{0.5})_{0.7}Ca_{0.3}Co_{0.8}Fe_{0.2}O_{3-\delta}$. At low temperature, oxygen permeation rate of composites were higher than BSCCF indicating high oxygen vacancies in the composite material therefore it may help to promote the reaction at low temperature.

Then, BSCCF, BSCCF: YSZ (3:1) composite fired at 1100°C for 10 hrs and BSCCF:GDC composites fired at 850°C for 10 hrs were chosen to study for impedance analysis and single cells testing because BSCCF: YSZ (3:1) composite has a higher

oxygen permeation rate than the composite fired for 9 hrs. And, BSCCF:GDC were chosen because they have no react phases after fired at 850˚C.

4.4 Impedance analysis of symmetric cell

4.4.1 $(Ba_{0.5}Sr_{0.5})_{0.7}Ca_{0.3}Co_{0.8}Fe_{0.2}O_{3-\delta}$ and the 3:1 composite of $(Ba_{0.5}Sr_{0.5})_{0.7}Ca_{0.3}Co_{0.8}Fe_{0.2}O_{3-\delta}$ and YSZ without the interlayer.

$(Ba_{0.5}Sr_{0.5})_{0.7}Ca_{0.3}Co_{0.8}Fe_{0.2}O_{3-\delta}$ and the composites fried at 1100℃ for 10 hrs were prepared for the symmetric cells: BSCCF//YSZ//BSCCF and BSCCF-YSZ(3:1)//YSZ// BSCCF-YSZ(3:1). The resistances of materials were measured at 850, 800, 750 and 700℃. For $(Ba_{0.5}Sr_{0.5})_{0.7}Ca_{0.3}Co_{0.8}Fe_{0.2}O_{3-\delta}$, the interfacial resistance increased when the temperature was decreased, as shown in Figure 4-9.

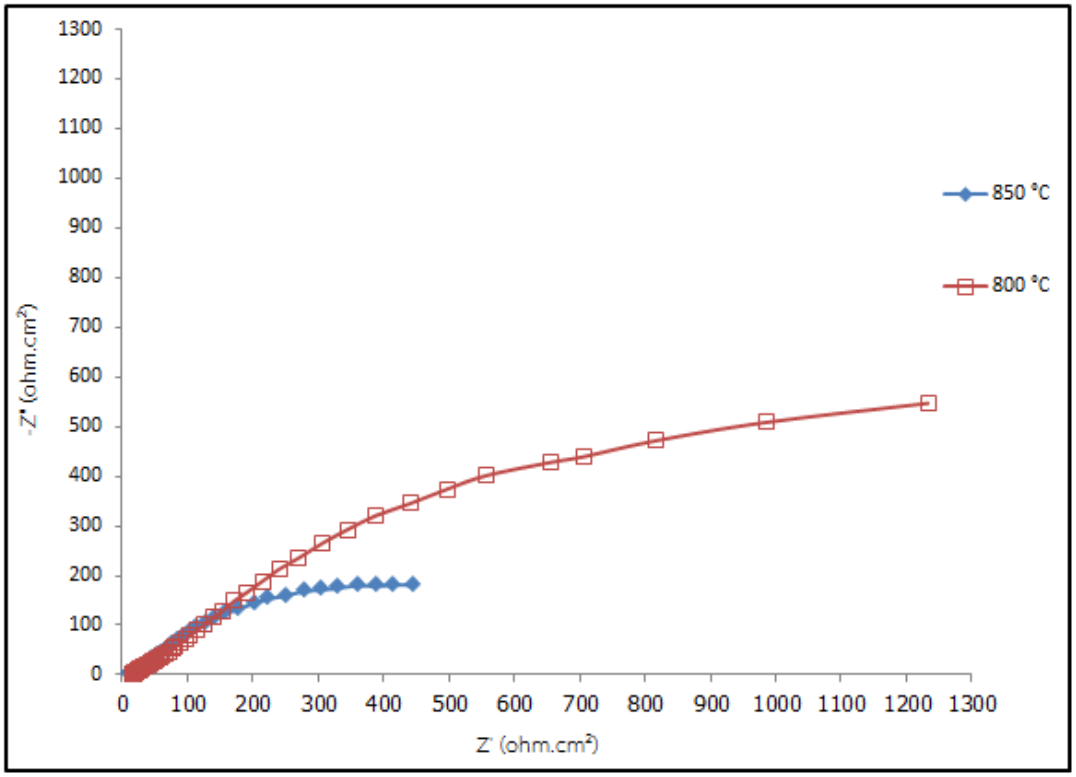

Figure 4-9 Impedance spectra of $(Ba_{0.5}Sr_{0.5})_{0.7}Ca_{0.3}Co_{0.8}Fe_{0.2}O_{3-\delta}$

The impedance spectra of $(Ba_{0.5}Sr_{0.5})_{0.7}Ca_{0.3}Co_{0.8}Fe_{0.2}O_{3-\delta}$ and the composite compound were displayed in Figure 4-10. The investigation showed the composite

has the higher ohmic and interfacial resistance than $(Ba_{0.5}Sr_{0.5})_{0.7}Ca_{0.3}Co_{0.8}Fe_{0.2}O_{3-\delta}$ at the same temperature. It can be explained by the composite material has contained impurity three phases, $Sr(ZrO_3)$, $SrCoO_3$ and unknown phase.

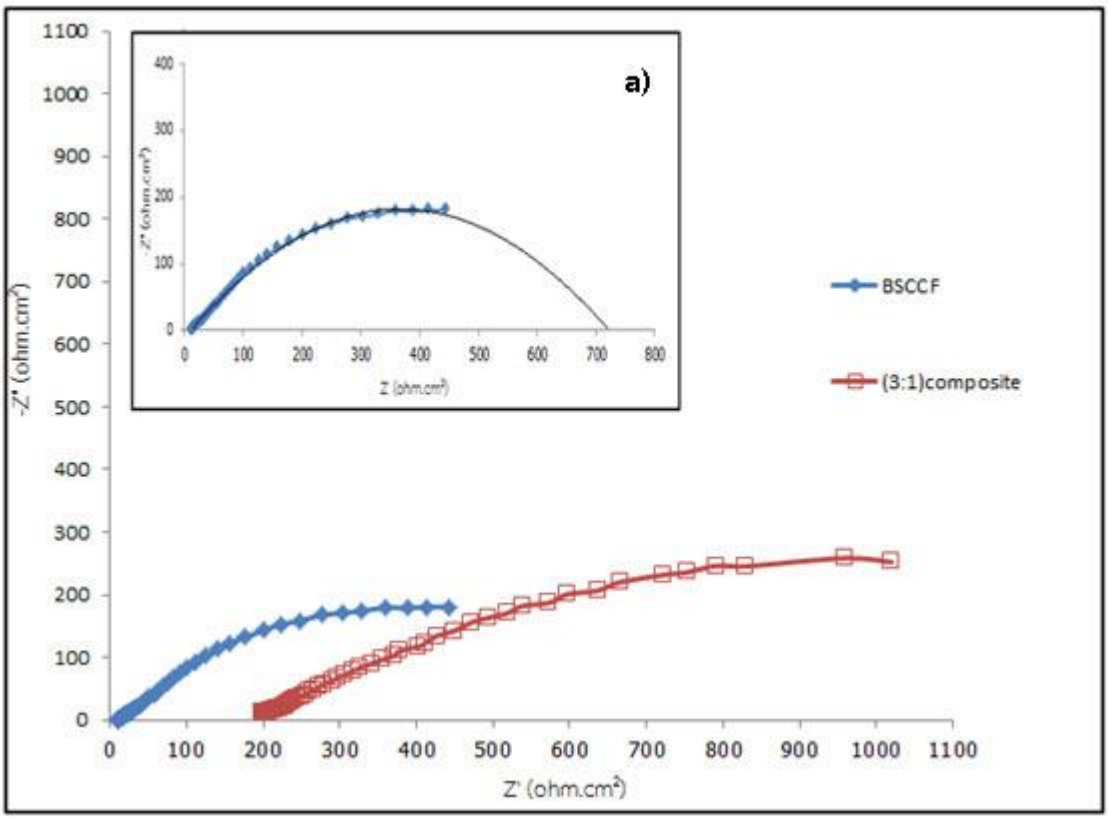

Figure 4-10 Impedance spectra of $(Ba_{0.5}Sr_{0.5})_{0.7}Ca_{0.3}Co_{0.8}Fe_{0.2}O_{3-\delta}$ and (3:1) composite at 850°C

Then, the activation energy (E_a) was determined from the slope of the Arrhenius plot, in Figure 4-11. The data on the Arrhenius plot were the interfacial resistances. The interfacial resistances were calculated from the difference between the real values (x-axis) of materials at high frequency and low frequency in the curve. Figure 4-10(a) showed a fitting curve from high to low frequency [41]. The interfacial resistances were plotted as a function of temperatures. The E_a of $(Ba_{0.5}Sr_{0.5})_{0.7}Ca_{0.3}Co_{0.8}Fe_{0.2}O_{3-\delta}$ is obtained around 8.02 kJ/mol while the E_a of composite is 14.058 kJ/mol. It can be suggested that the $(Ba_{0.5}Sr_{0.5})_{0.7}Ca_{0.3}Co_{0.8}Fe_{0.2}O_{3-\delta}$ will be a good cathode in SOFC better than the composite.

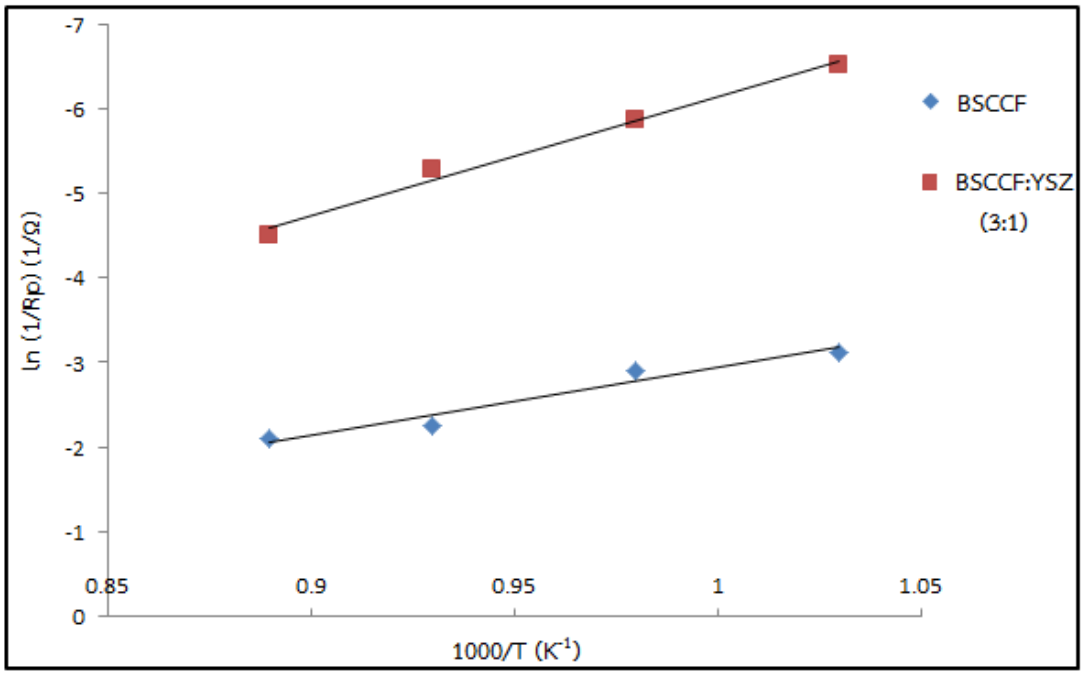

Figure 4-11 The Arrhenius plot of BSCCF and BSCCF:YSZ(3:1) at 850, 800, 750, 700°C

4.4.2 $(Ba_{0.5}Sr_{0.5})_{0.7}Ca_{0.3}Co_{0.8}Fe_{0.2}O_{3-\delta}$ and the composites of $(Ba_{0.5}Sr_{0.5})_{0.7}Ca_{0.3}Co_{0.8}Fe_{0.2}O_{3-\delta}$ and GDC with the interlayer

The resistances of $(Ba_{0.5}Sr_{0.5})_{0.7}Ca_{0.3}Co_{0.8}Fe_{0.2}O_{3-\delta}$ and the BSCCF:GDC composite in symmetric cell were measured at 850, 800, 750 and 700°C. Figure 4-12 shows the composites in 3:1, 1:1 and 1:3 have higher ohmic and interfacial resistance than $(Ba_{0.5}Sr_{0.5})_{0.7}Ca_{0.3}Co_{0.8}Fe_{0.2}O_{3-\delta}$ at 850°C. The high resistance of the composite could be come from the increasing of the GDC ratio in the composites because GDC electrolyte has low electronic conductivity.

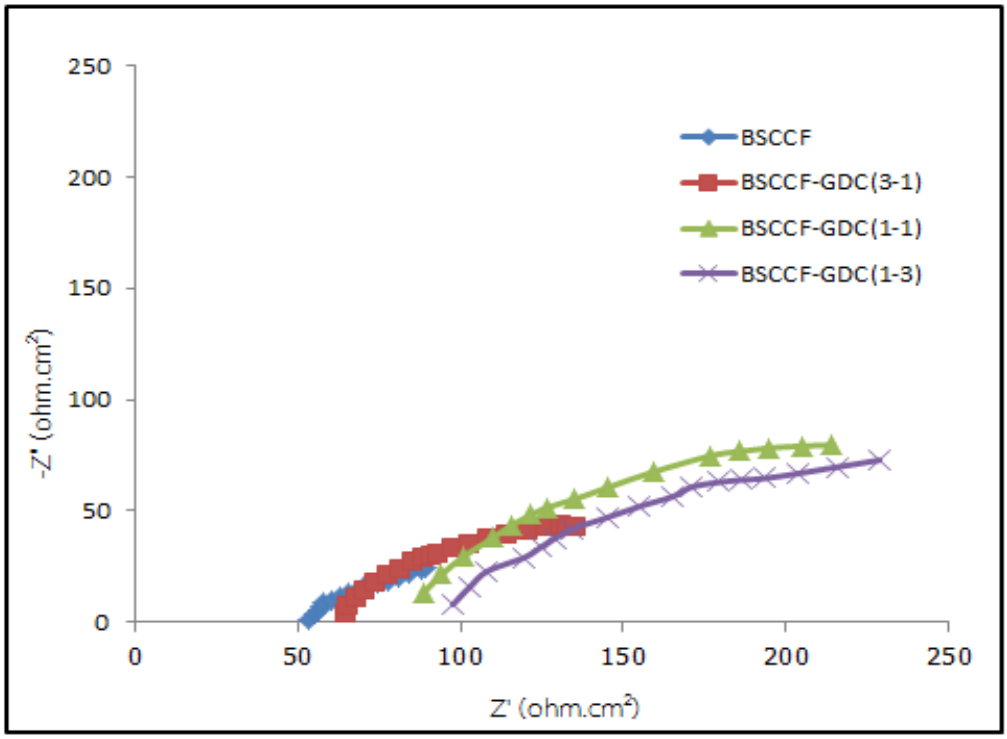

Figure 4-12 Impedance spectra of $(Ba_{0.5}Sr_{0.5})_{0.7}Ca_{0.3}Co_{0.8}Fe_{0.2}O_{3-\delta}$ and composites with the GDC interlayer at 850°C

The Arrhenius plot was calculated using the data from the interfacial resistance and displayed in Figure 4-13. The activation energy (E_a) was calculated from the slope of the Arrhenius plot. The E_a values of $(Ba_{0.5}Sr_{0.5})_{0.7}Ca_{0.3}Co_{0.8}Fe_{0.2}O_{3-\delta}$ and the composite

in 3:1, 1:1 and 1:3 weight ratio are 25.94, 15.51, 19.46 and 17.10 kJ/mol, respectively.

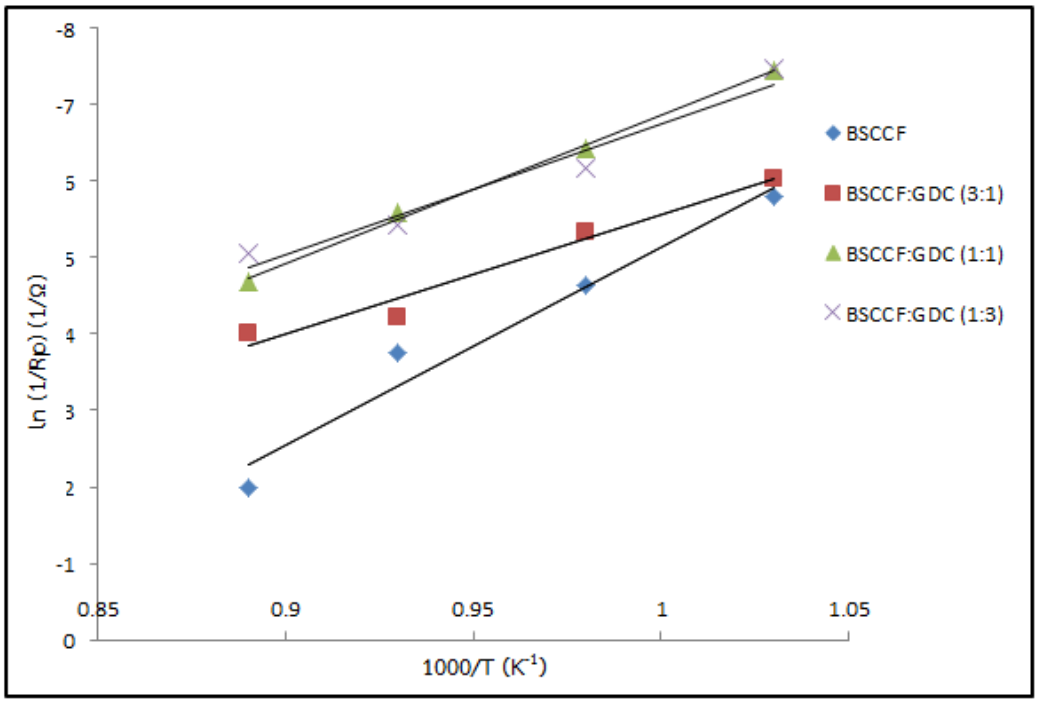

Figure 4-13 The Arrhenius plot of at 850, 800, 750, 700°C

4.5 Single cell performance of cathode materials

4.5.1 $(Ba_{0.5}Sr_{0.5})_{0.7}Ca_{0.3}Co_{0.8}Fe_{0.2}O_{3-\delta}$ and the composite without GDC interlayer

$(Ba_{0.5}Sr_{0.5})_{0.7}Ca_{0.3}Co_{0.8}Fe_{0.2}O_{3-\delta}$ and the 3:1 composite fired at 1100°C for 10 hrs were measured for the single cell performance. The performance test of BSCCF//YSZ//Ni-YSZ was shown in Figure 4-14. The power density for the single cell was decreased when the temperature decreased from 850°C to 800°C. The maximum power density of material was achieved for 5.56 mW/cm^{-2} at 850°C but the power density could not be detected at 750°C. The performance is very low because the reactivity between the interface of the electrolyte and the cathode occurs to produce $Sr(ZrO_3)$ which is in agreement with the XRD analysis. For the single cell performance test of BSCCF-YSZ(3:1)//YSZ//Ni-YSZ at 850- 650°C, the power density is too low to be detected which may be the composite contains of $Sr(ZrO_3)$ and $SrCoO_3$ phases. Then, $(Ba_{0.5}Sr_{0.5})_{0.7}Ca_{0.3}Co_{0.8}Fe_{0.2}O_{3-\delta}$ and the composite BSCCF : YSZ (3:1) may

be not suitable for used with YSZ electrolyte because the reaction between the cathode materials and electrolyte leading low power densities.

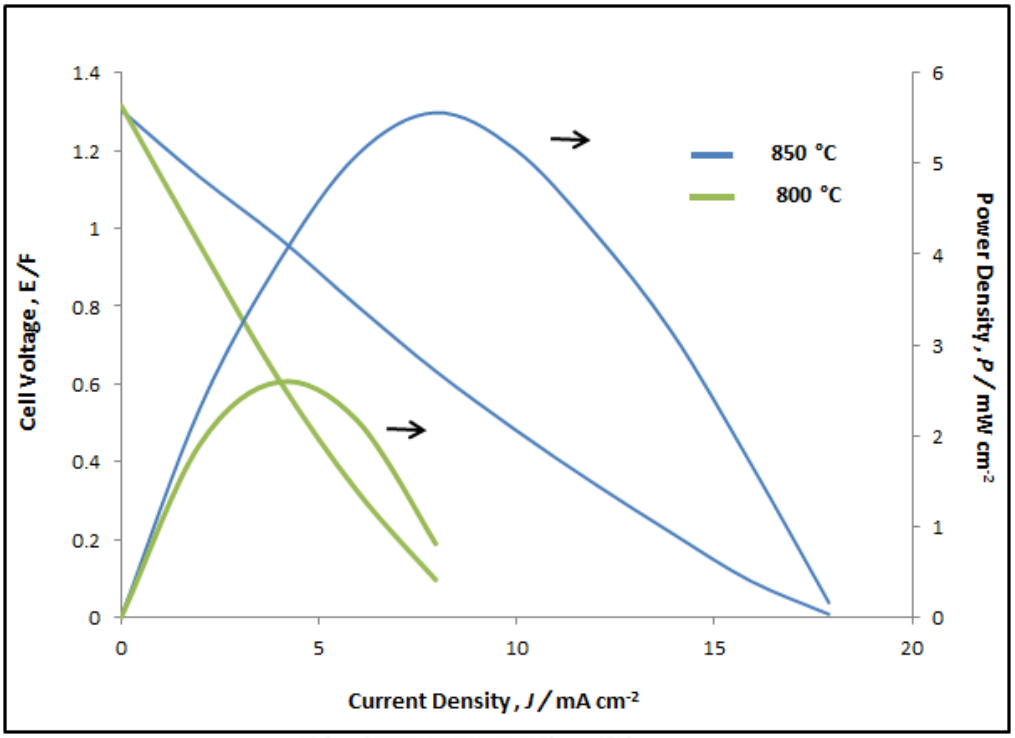

Figure 4-14 The cell performance of BSCCF//YSZ//Ni-YZS

4.5.2 $(Ba_{0.5}Sr_{0.5})_{0.7}Ca_{0.3}Co_{0.8}Fe_{0.2}O_{3-\delta}$ and the composite of $(Ba_{0.5}Sr_{0.5})_{0.7}Ca_{0.3}Co_{0.8}Fe_{0.2}O_{3-\delta}$ and GDC electrolyte with GDC interlayer

The single cell performance test of BSCCF//GDC//YSZ//Ni-YZS was shown in Figure 4-15. The maximum power density of material was achieved for 163.84 mW/cm^{-2} at 850°C and decreased when the temperature went down. The single cell performance test of BSCCF:GDC (3:1)//GDC//YSZ//Ni-YZS at 850- 650°C was also shown in Figure 4-16. The maximum power density was detected as 96.00 mW/cm^{-2}. Then, the maximum power density was also decreased when the temperature went down. In Figure 4-17, the cell performance of BSCCF:GDC (1:1)//GDC//YSZ//Ni-YZS single cell shows the highest power density as 59.23 mW/cm^{-2} at 850°C. The power density of BSCCF:GDC (1:3)//GDC//YSZ//Ni-YZS single cell could not be detected because the composite has contained GDC more than the 3:1 and 1:1 composites. GDC has low conductivity so the power density has been decreased with increasing the GDC ratio in the composites. Figure 4-18 shows the comparison in the maximum

power density of single cells between BSCCF, BSCCF:GDC (3:1), BSCCF:GDC (1:1) at 850°C, suggesting BSCCF may be a potential cathode in SOFC.

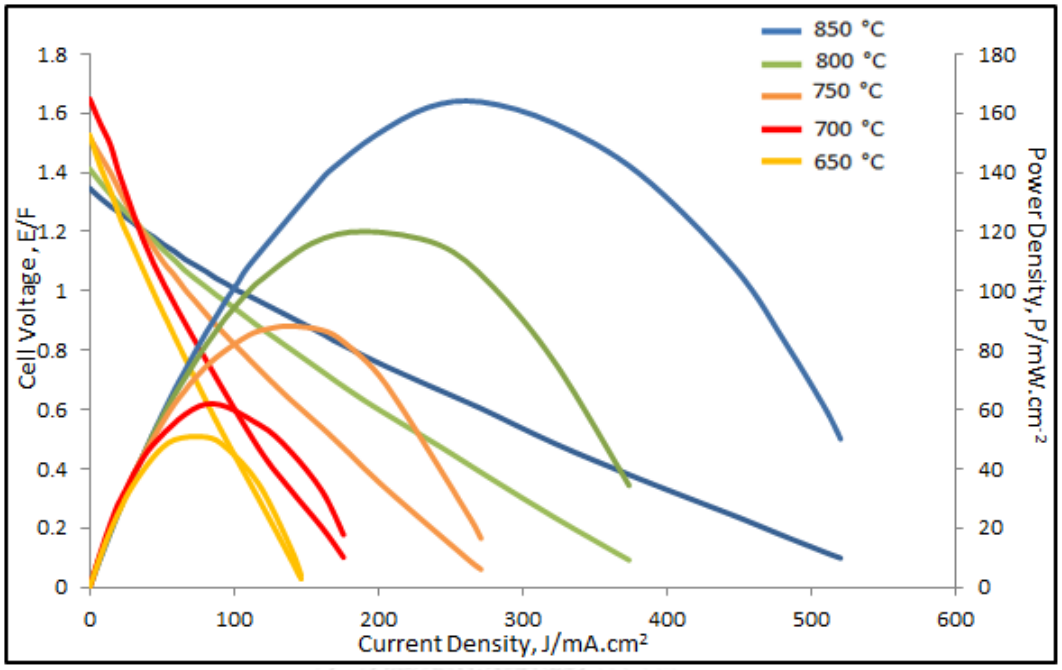

Figure 4-15 The cell performance of BSCCF//GDC//YSZ//Ni-YZS

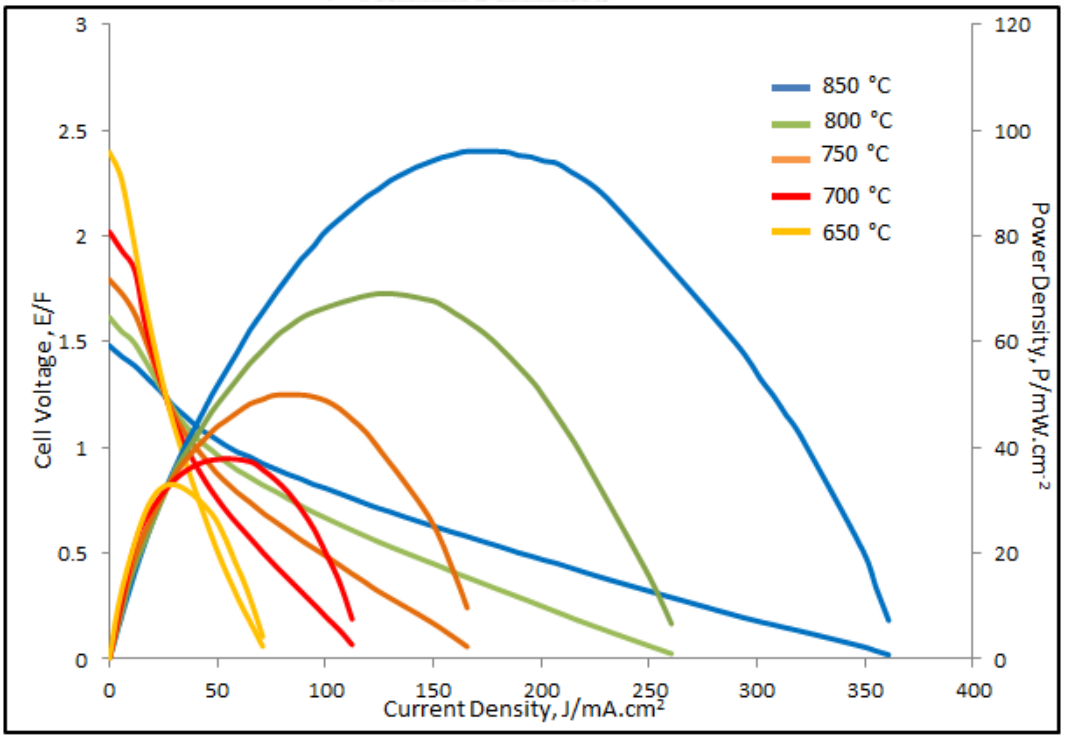

Figure 4-16 The cell performance of BSCCF:GDC (3:1)//GDC//YSZ//Ni-YZS

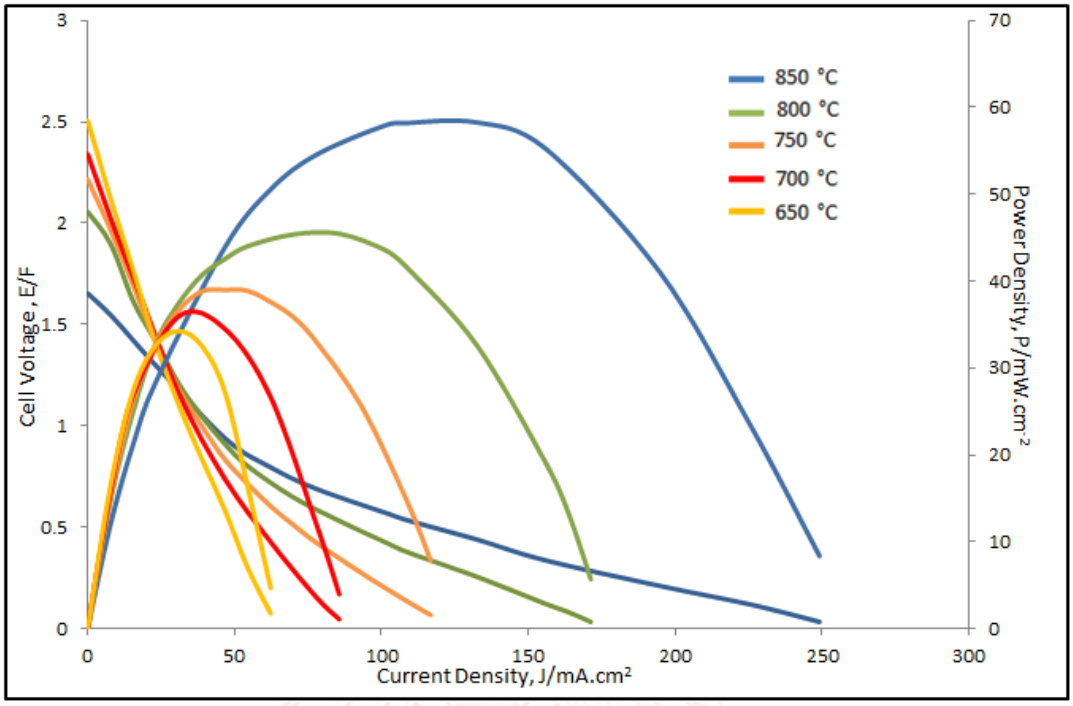

Figure 4-17 The cell performance of BSCCF:GDC(1-1)//GDC//YSZ//Ni-YZS

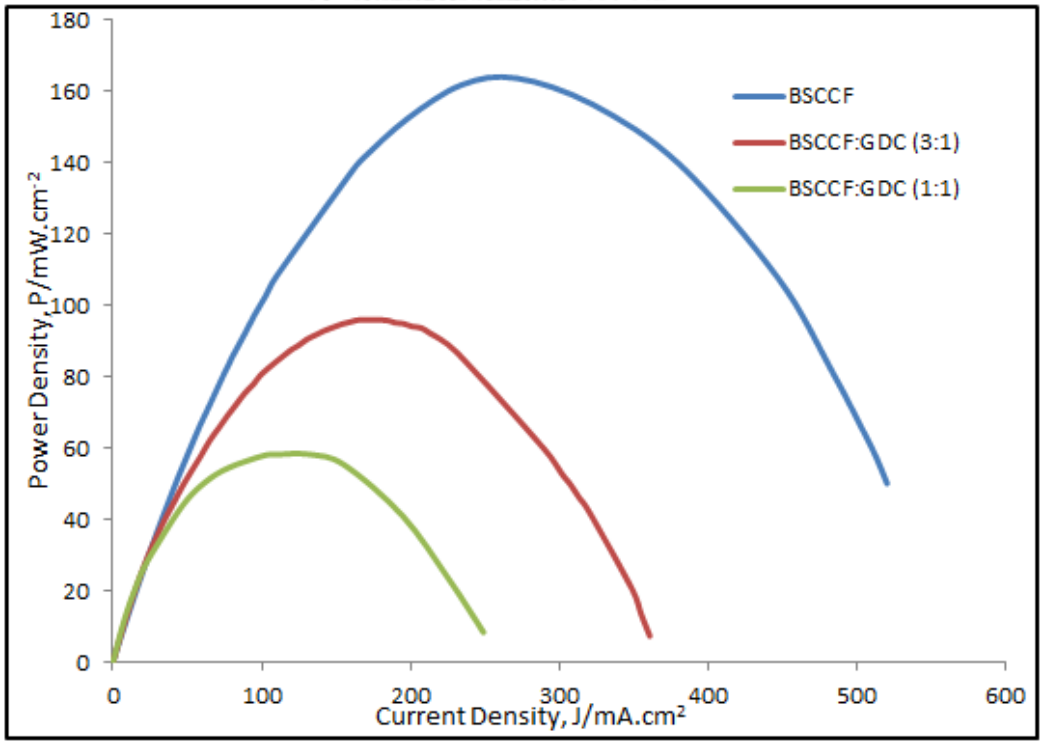

Figure 4-18 The power densities of the single cell at 850°C

From the result of single cell test with and without the GDC interlayer between the cathodes and the electrolyte, the single cell performance test with the

GDC interlayer gave a higher power density because GDC interlayer prevent the reactivity between the cathodes and YSZ electrolyte disc. Unwanted phases did not occur at the interphase between the interfacial. It could be suggested that the cell performance test of $(Ba_{0.5}Sr_{0.5})_{0.7}Ca_{0.3}Co_{0.8}Fe_{0.2}O_{3-\delta}$ should have the GDC interlayer to obtain the highest power density.

4.6 Impedance analysis of the single cells

4.6.1 $(Ba_{0.5}Sr_{0.5})_{0.7}Ca_{0.3}Co_{0.8}Fe_{0.2}O_{3-\delta}$ and the composite of $(Ba_{0.5}Sr_{0.5})_{0.7}Ca_{0.3}Co_{0.8}Fe_{0.2}O_{3-\delta}$ and YSZ without GDC interlayer

The ac impedance studies of both single cells from 4.5 were investigated and the spectra were shown in Figures 4-19 and 4-20. The polarization resistance for the single cell of BSCCF//YSZ//Ni-YSZ was lower than that of BSCCF:YSZ(3:1)//YSZ//Ni-YSZ at the same temperature. This result can be explained the single cell performance of BSCCF-YSZ(3:1)//YSZ//Ni-YSZ, which could not be detected due to the high polarization resistance. Figure 4-21 indicates the polarization resistances of BSCCF//YSZ//Ni-YSZ was increased when the measuring temperature was decreased. This corresponds to the cell performance test at high temperature is better than at low temperature.

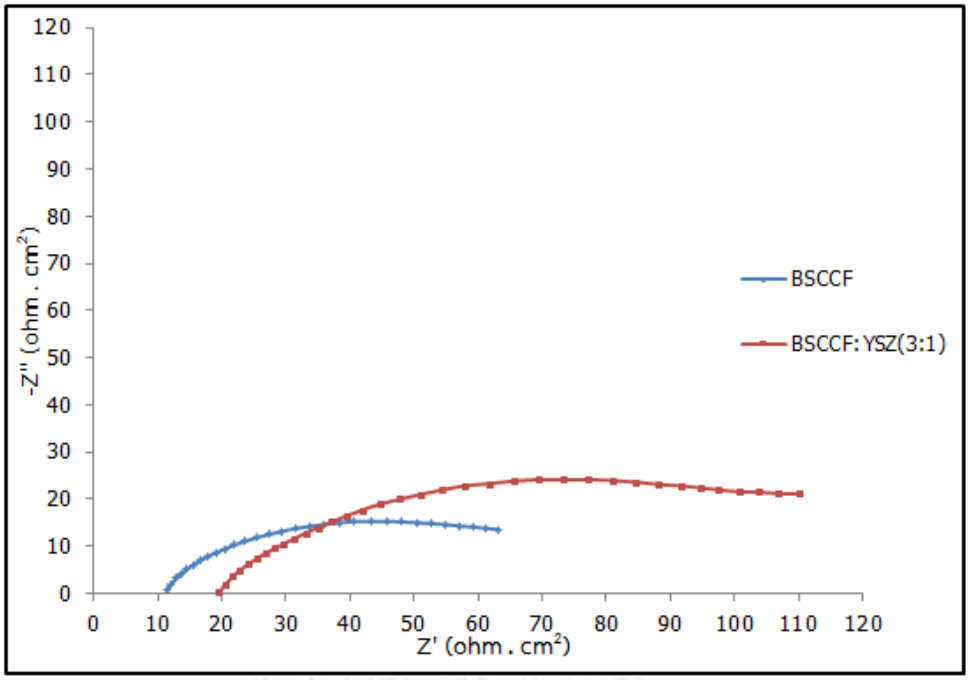

Figure 4-19 The ac impedance spectra of BSCCF//YSZ//NiO-YSZ cell and BSCCF:YSZ(3:1)//YSZ//NiO-YSZ at 850°C

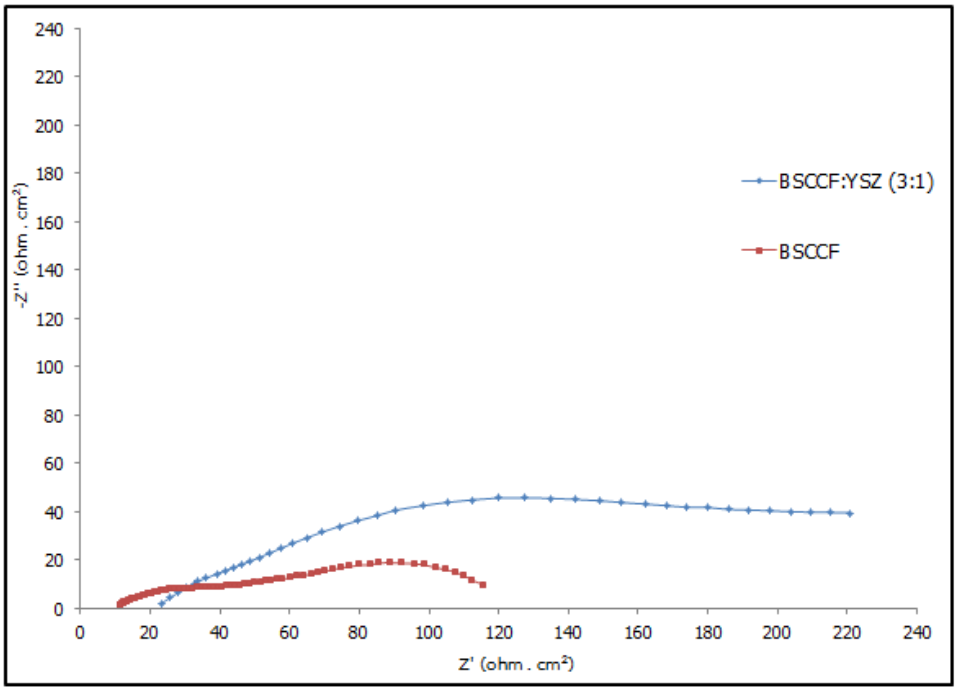

Figure 4-20 The ac impedance spectra of BSCCF//YSZ//NiO-YSZ and BSCCF:YSZ(3:1)//YSZ//NiO-YSZ at 800 °C

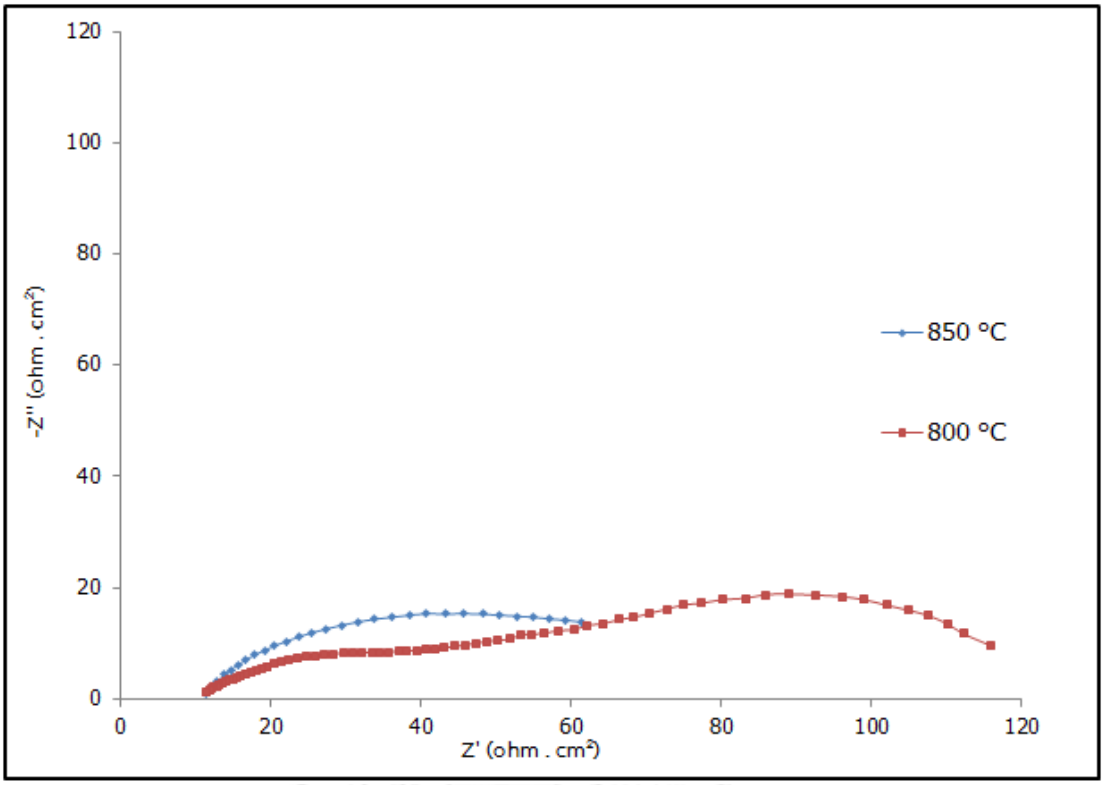

Figure 4-21 The ac impedance spectra of BSCCF//YSZ//NiO-YSZ single cell

4.6.2 $(Ba_{0.5}Sr_{0.5})_{0.7}Ca_{0.3}Co_{0.8}Fe_{0.2}O_{3-\delta}$ and the composite of $(Ba_{0.5}Sr_{0.5})_{0.7}Ca_{0.3}Co_{0.8}Fe_{0.2}O_{3-\delta}$ and GDC with GDC interlayer

The ac impedance studies of single cells were shown in Figures 4-22, 4-23 and 4-24. Similar to the resistances in 4.6.1, the resistances of single cells were increased when the measuring temperature was decreased, leading to the cell performance test at high temperature was better than low temperature. Figure 4-25 shows the comparison in polarization resistances of the single cells at 850°C. The resistances of the studied cell are in the following order: BSCCF< BSCCF:GDC(3:1) < BSCCF:GDC(1:1) which relates to the single cell performance BSCCF > BSCCF:GDC(3:1) > BSCCF:GDC(1:1).

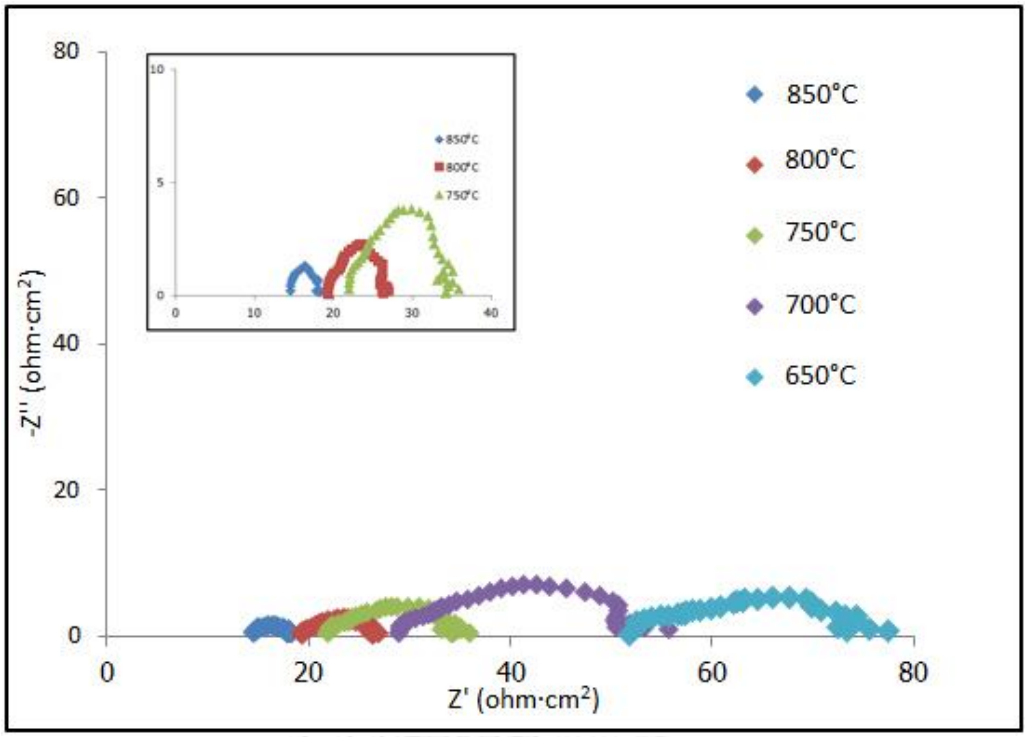

Figure 4-22 The ac impedance spectra of BSCCF//GDC//YSZ//Ni-YZS

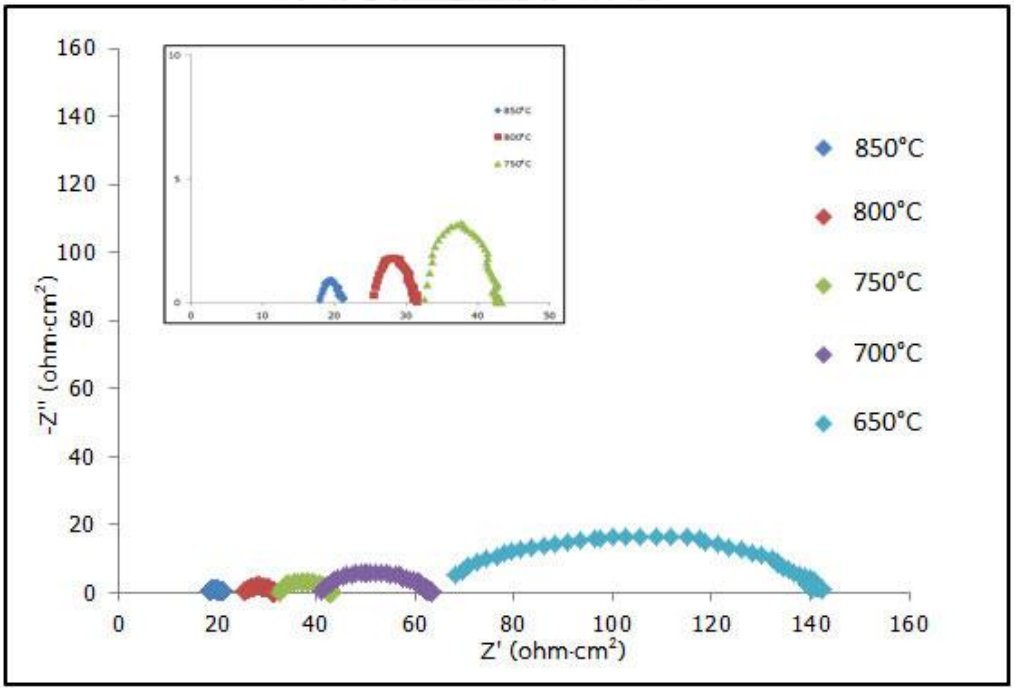

Figure 4-23 The ac impedance spectra of BSCCF-GDC(3:1)//GDC//YSZ//Ni-YZS

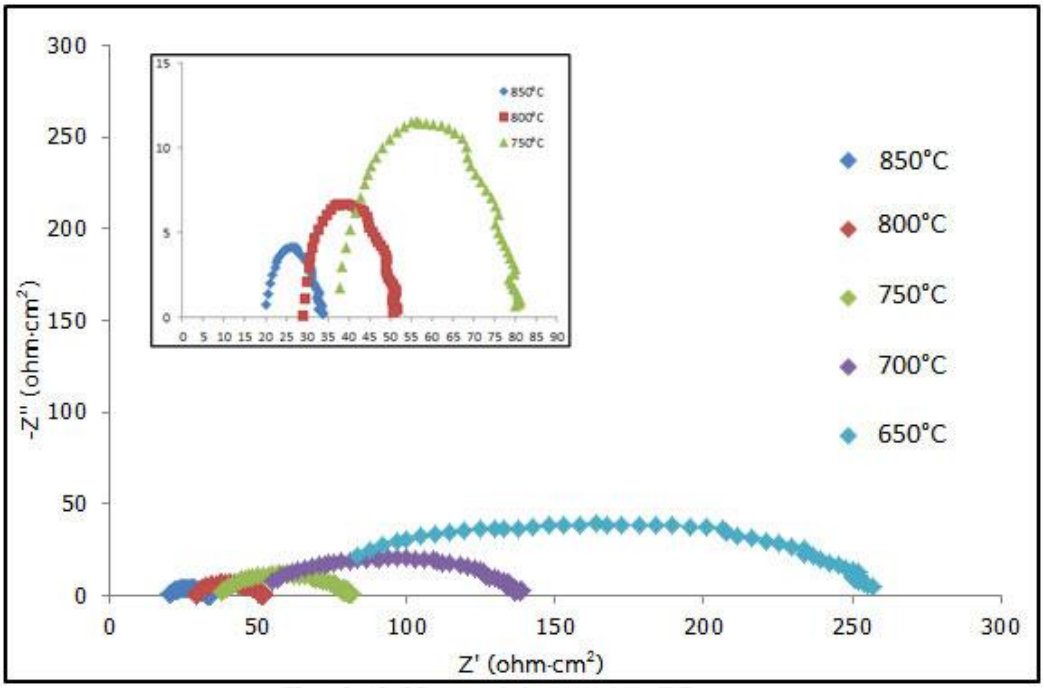

Figure 4-24 The ac impedance spectra of BSCCF-GDC(1:1)//GDC//YSZ//Ni-YZS

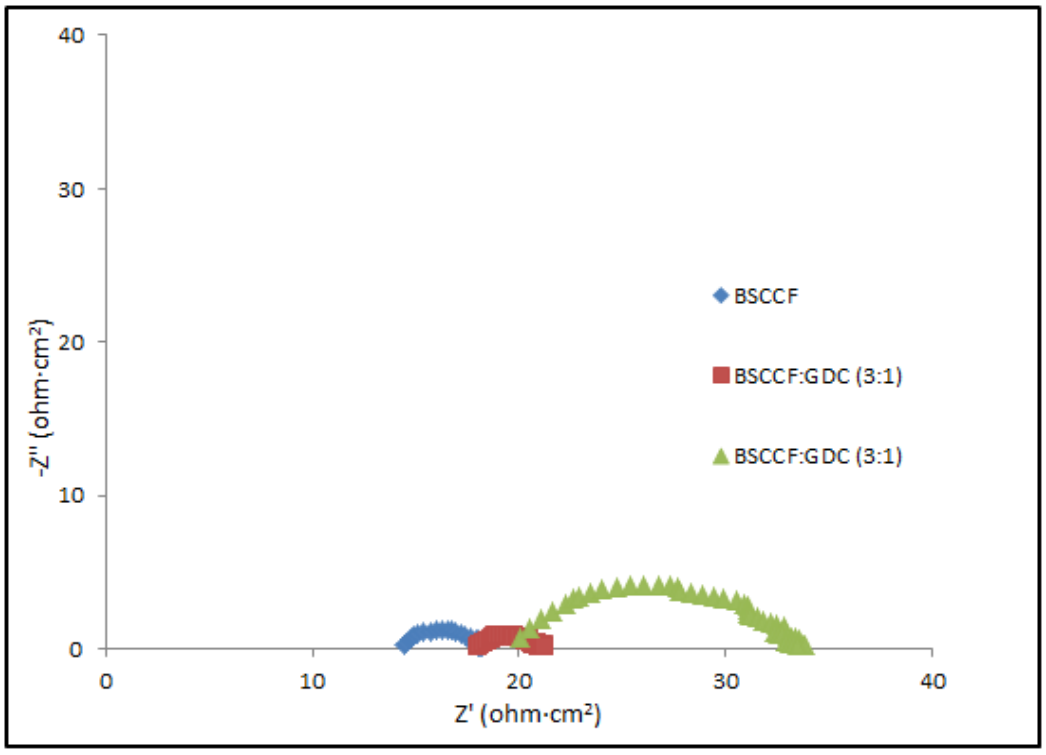

Figure 4-25 The ac impedance spectra of single cells at 850°C

4.7 The morphology

The morphology of single cells were studied for the surface and the cross-section of the single cell.

4.7.1 The surface analysis

4.7.1.1 $(Ba_{0.5}Sr_{0.5})_{0.7}Ca_{0.3}Co_{0.8}Fe_{0.2}O_{3-\delta}$ and the composite of $(Ba_{0.5}Sr_{0.5})_{0.7}Ca_{0.3}Co_{0.8}Fe_{0.2}O_{3-\delta}$ and YSZ (1:3) without GDC interlayer

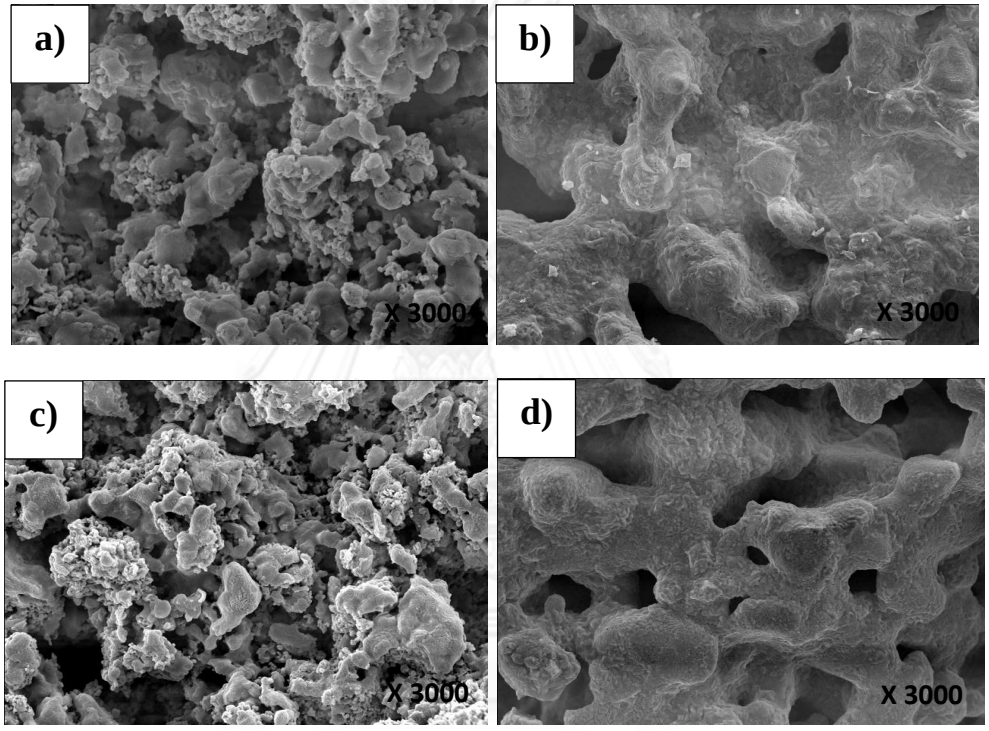

Figure 4-26. Surface microstructures of $(Ba_{0.5}Sr_{0.5})_{0.7}Ca_{0.3}Co_{0.8}Fe_{0.2}O_{3-\delta}$ (a) before testing, (b) after testing; and the composite (c) before testing, (d) after testing, without interlayer

Figure 4-26 shows the surface morphology of $(Ba_{0.5}Sr_{0.5})_{0.7}Ca_{0.3}Co_{0.8}Fe_{0.2}O_{3-\delta}$ and the composite of $(Ba_{0.5}Sr_{0.5})_{0.7}Ca_{0.3}Co_{0.8}Fe_{0.2}O_{3-\delta}$ and YSZ electrolyte (1:3) without the interlayer. The morphology of the cathodes after the single cell testing was changed. The cathodes after the cell test were melted and more densified than those before the cell testing. The change in particle size and property may prohibit the transport of oxide ions to the electrolyte. It is also leading to the low density of cell performance test for single cell without the GDC interlayer.

4.7.1.2 $(Ba_{0.5}Sr_{0.5})_{0.7}Ca_{0.3}Co_{0.8}Fe_{0.2}O_3$ and the composite of $(Ba_{0.5}Sr_{0.5})_{0.7}Ca_{0.3}Co_{0.8}Fe_{0.2}O_{3-\delta}$ and GDC with interlayer

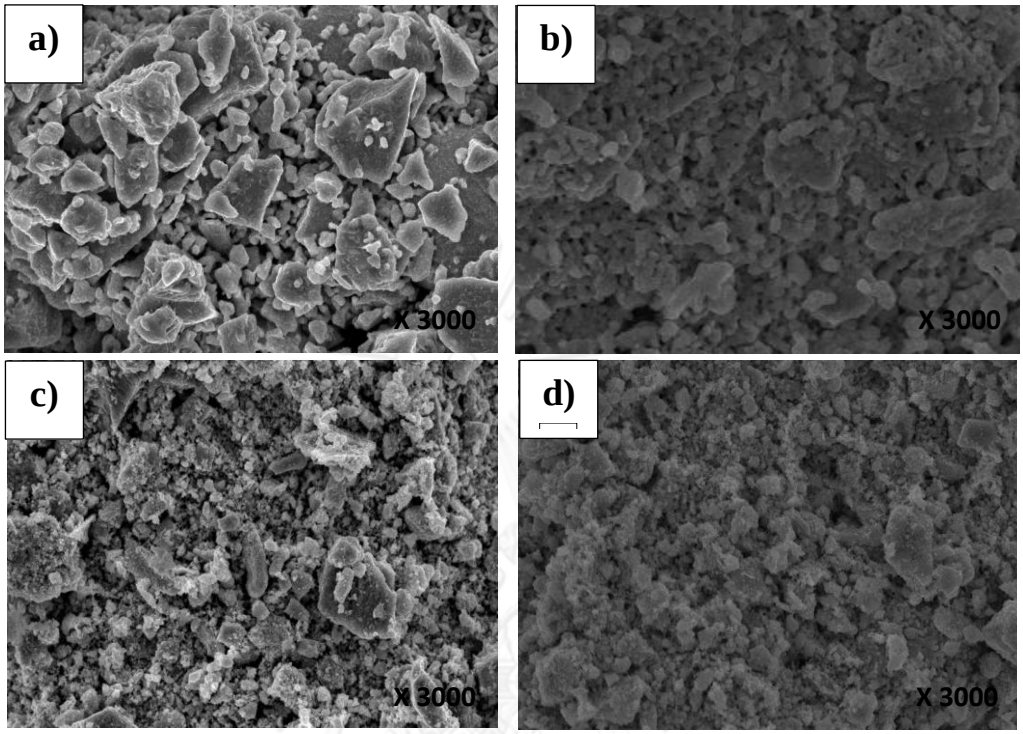

Figure 4-27 Surface microstructures of $(Ba_{0.5}Sr_{0.5})_{0.7}Ca_{0.3}Co_{0.8}Fe_{0.2}O_{3-\delta}$ (a) before testing, (b) after testing; and the composite (c) before testing, (d) after testing, with the interlayer

The surface morphology of $(Ba_{0.5}Sr_{0.5})_{0.7}Ca_{0.3}Co_{0.8}Fe_{0.2}O_{3-\delta}$ and the composite (3:1) have shown in Figure 4-27. Morphology of both of cathodes after the single cell testing were not changed, which suggests no interaction occurs between cathode and electrolyte. In addition, GDC works as an active interlayer in this study.

4.7.2 Cross section analysis

4.7.2.1. $(Ba_{0.5}Sr_{0.5})_{0.7}Ca_{0.3}Co_{0.8}Fe_{0.2}O_3$ and the composite of $(Ba_{0.5}Sr_{0.5})_{0.7}Ca_{0.3}Co_{0.8}Fe_{0.2}O_{3-\delta}$ and YSZ without interlayer

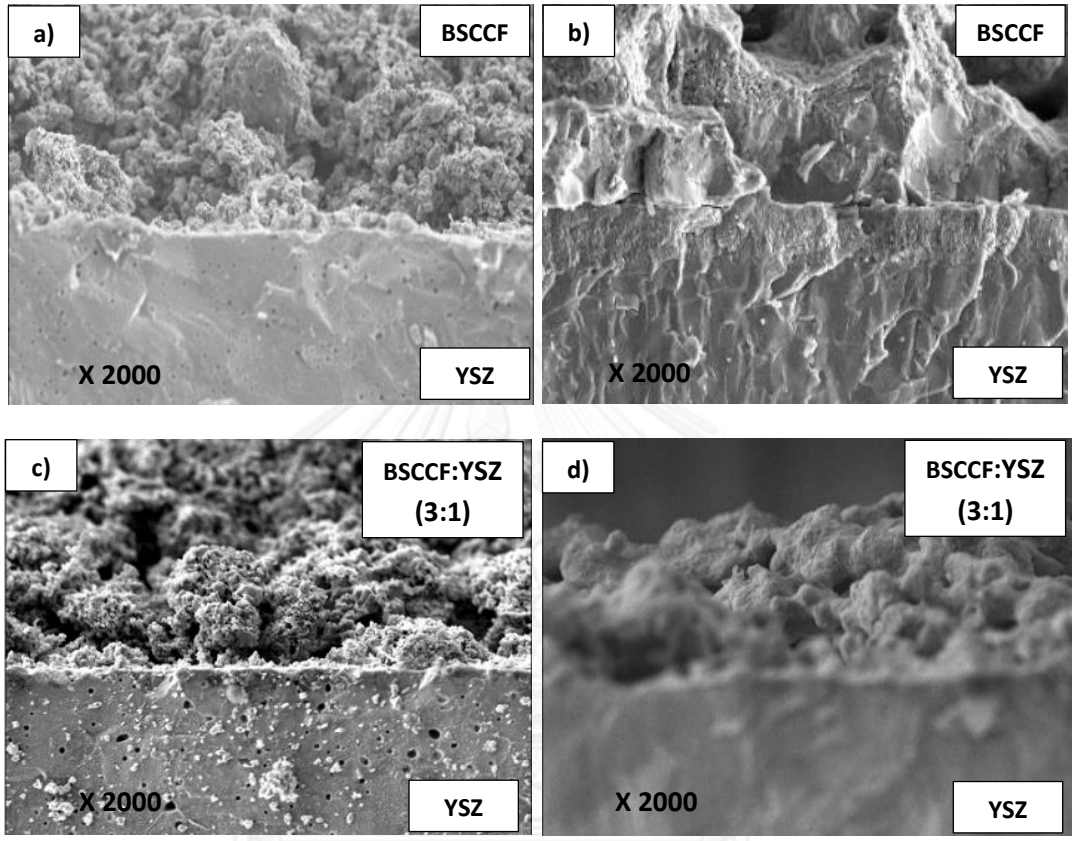

Figure 4-28 The cross section of cell fabrication on BSCCF//YSZ (a) before testing, (b) after testing and on BSCCF-YSZ(3:1)//YSZ (c) before testing, (d) after testing.

The cross-section of cell fabrications of $(Ba_{0.5}Sr_{0.5})_{0.7}Ca_{0.3}Co_{0.8}Fe_{0.2}O_{3-\delta}$ and the composite as cathode with YSZ electrolyte disc were shown on the Figure 4-28. The cross-sections show the connection between the cathode side and the electrolyte. The bulk cathode materials after the cell testing showed the change in particle size of cathode materials.

4.7.2.3. $(Ba_{0.5}Sr_{0.5})_{0.7}Ca_{0.3}Co_{0.8}Fe_{0.2}O_3$ and the composite of $(Ba_{0.5}Sr_{0.5})_{0.7}Ca_{0.3}Co_{0.8}Fe_{0.2}O_{3-\delta}$ and GDC with interlayer

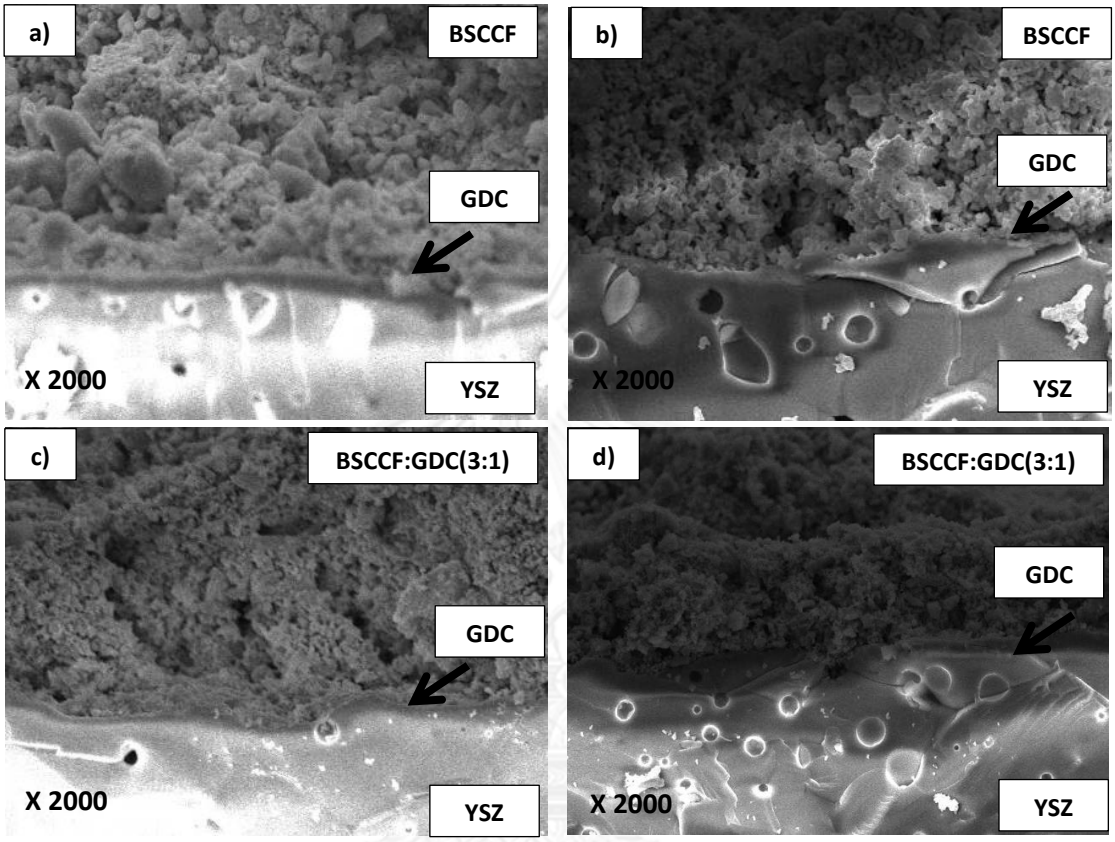

Figure 4-29 The cross section of cell fabrication on BSCCF//GDC//YSZ (a) before testing , (b) after testing and on BSCCF:GDC(3:1)//GDC//YSZ (c) before testing, (d) after testing.

Figure 4-29 shows the cross-section from cell fabrications of $(Ba_{0.5}Sr_{0.5})_{0.7}Ca_{0.3}Co_{0.8}Fe_{0.2}O_{3-\delta}$ and the GDC composite (3:1) as cathodes with the GDC interlayer. The cross-section images show the fine connection between the cathode side and the electrolyte by the interlayer. The morphology of the cathodes after the testing did not change comparing to the cathodes before the single cell test. It could be related with the high power density because the interlayer can protect the reaction between the cathodes and YSZ electrolyte disc, and no delamination occurs along the interface.

CHARTER V
CONCLUSION AND SUGGESTION

5.1 Conclusion

The composite of $(Ba_{0.5}Sr_{0.5})_{0.7}Ca_{0.3}Co_{0.8}Fe_{0.2}O_{3-\delta}$ with YSZ and GDC electrolyte in weight ratio of 1:3, 1:1 and 3:1 were fired at 850 – 1,300°C for 7-10 hrs. XRD analysis of phase structures indicated the BSCCF:YSZ composite after firing produced $SrZrO_3$, $CaZrO_3$ and $SrCoO_3$ as new phases. The BSCCF:GDC composite fired at 850 °C found only BSCCF and GDC structures, but the composite fired above 900°C gave $SrCoO_3$ structure.

The electrical conductivity could be obtained from $(Ba_{0.5}Sr_{0.5})_{0.7}Ca_{0.3}Co_{0.8}Fe_{0.2}O_{3-\delta}$ and the BSCCF:YSZ (3:1) composites fried at 1100°C for 7-10 hrs, 1000°C for 10 hrs only. $(Ba_{0.5}Sr_{0.5})_{0.7}Ca_{0.3}Co_{0.8}Fe_{0.2}O_{3-\delta}$ showed the highest elctrical conductivity while the composites performed very low conductivity because the poor conductivity of unwanted phases; $SrZrO_3$, $CaZrO_3$ and $SrCoO_3$. Additionally, $(Ba_{0.5}Sr_{0.5})_{0.7}Ca_{0.3}Co_{0.8}Fe_{0.2}O_{3-\delta}$ showed the highest oxygen permeation rate at 850°C and decreased with temperature.

On the comparison of the symmetric cell resistances, $(Ba_{0.5}Sr_{0.5})_{0.7}Ca_{0.3}Co_{0.8}Fe_{0.2}O_{3-\delta}$ without the GDC interlayer is a poor single cell because it exhibited higher interfacial resistances than the one with the GDC innterlayer. The single cell performance of BSCCF without the GDC interlayer was very low in power density whereas that with the GDC interlayer was as highly as 163.84 mW/cm^{-2} at 850°C for the BSCCF//GDC//YSZ//Ni-YSZ. This is because the GDC interlayer prevents the reaction between the cathode material and YSZ electrolyte disc. The polarization resistances of the single cells without the GDC interlayer were higher than the single cells with the GDC interlayer. The results were consistent with the single cell performance. The morphology on surface and cross-section of the cell of $(Ba_{0.5}Sr_{0.5})_{0.7}Ca_{0.3}Co_{0.8}Fe_{0.2}O_{3-\delta}$ and the composite of BSCCF:YSZ single cell without the GDC interlayer were changed after the cell testing because the reactivity between

$(Ba_{0.5}Sr_{0.5})_{0.7}Ca_{0.3}Co_{0.8}Fe_{0.2}O_{3-\delta}$ and YSZ. On the contrary, $(Ba_{0.5}Sr_{0.5})_{0.7}Ca_{0.3}Co_{0.8}Fe_{0.2}O_{3-\delta}$ and the composite of BSCCF:GDC single cell with the GDC interlayer remained unchanged.

From this work, $(Ba_{0.5}Sr_{0.5})_{0.7}Ca_{0.3}Co_{0.8}Fe_{0.2}O_{3-\delta}$ material cannot be used as a cathode when directly equipped with the YSZ electrolyte because $(Ba_{0.5}Sr_{0.5})_{0.7}Ca_{0.3}Co_{0.8}Fe_{0.2}O_{3-\delta}$ will react with YSZ. However, when GDC is used as an interlayer to prevent the reaction between $(Ba_{0.5}Sr_{0.5})_{0.7}Ca_{0.3}Co_{0.8}Fe_{0.2}O_{3-\delta}$ and some BSCCF:GDC cathodes and YSZ, the cell performance can be achieved.

5.2 Suggestion for the further work

1. The single cell performance should be tested for a long time period to study the stability of the cathodes.

2. The single cell should be tested for the voltage loss in the cathode materials.

REFERENCES

[1] Ecology global network.. Available from: http://www.ecology.com/2011/09/06/fossil-fuels-vs-renewable-energy-resources/

[2] Environmental Protection Agency. Available from: http://www.policyalmanac.org/environment/archive/acid_rain.shtml

[3] Alternative Energy Sources. Available from: http://saveenergy.about.com/od/alternativeenergysources/.

[4] Solid oxide fuel cells.; Available from: http://www.csa.com/discoveryguides/fuecel/overview.php#n1.

[5] Singhal, S., High-temperature Solid Oxide Fuel Cells: Fundamentals, Design and Applications. 2003: Elsevier.

[6] Zongping S, S. A high-performance cathode for the next generation of solid-oxide fuel cells.pdf. Nature, 2004: p. 170-173.

[7] Deehasing, S., et al., Influence of Cation Dopants in the A-Site on the Crystal Structure, Microstructure, and Electrical Conductivity of $Ba_{0.5}Sr_{0.5}Co_{0.8}Fe_{0.2}O_{3-\delta}$ as a New Solid-Oxide-Fuel-Cell Cathode. Japanese Journal of Applied Physics, 2011. **50**: p. 01BF06.

[8] Hyung-Ryul, R., Euney, J., Ju-Seong, L. Characteristics of $Pr_{1-x}M_xMnO_3$ (M = Ca, Sr) as cathode material in solid oxide fuel cells. Materials Chemistry and Physics 1998. **52**: p. 54-59.

[9] Tu, H.Y., Yang, Y.J., Lu, Z.Y., Wang, D.Q., Wen, T.L. Chemical compatibility of $RE_{0.6}M_{0.4}Mn_{0.8}Co_{0.2}O_{3-\delta}$ (RE=La, Pr,Nd, Sm and Gd; M=Sr and Ca) with yttria stabilized zirconia. Journal of the European Ceramc Society, 2000. **20**: p. 2421-2425.

[10] Kostogloudis, G.Ch., Ftikos, C. Chemical reactivity of perovskite oxide SOFC cathodes and yttria stabilized zirconia. Solid State Ionics, 2000. **135**: p. 529-525.

[11] Suna, K., Zhang, N., Chen, X., Xu, S., Zhou, D. Fabrication and performance of $La_{0.8}Sr_{0.2}MnO_3$/YSZ graded composite cathodes for SOFC. Rare Metal, 2008. **27**(3): p. 278-281.

[12] Huang, X., et al., Preparation and characteristics of $Pr_{1.6}Sr_{0.4}NiO_4$+YSZ as composite cathode of solid oxide fuel cells. Journal of Physics and Chemistry of Solids, 2009. **70**(3-4): p. 665-668.

[13] Tu, H.Y., Yang, Y.J., Lu, Z.Y., Wang, D.Q., Wen, T.L. Chemical compatibility of $RE_{0.6}M_{0.4}Mn_{0.8}Co_{0.2}O_{3-\delta}$ (RE=La, Pr,Nd, Sm and Gd; M=Sr and Ca) with yttria stabilized zirconia. Journal of the European Ceramc Society, 2000. **20**: p. 2421-2425.

[14] Qingshanzhu, T. Thermal expansion behavior and chemical compatibility of $Ba_xSr_{1-x}Co_{1-y}Fe_yO_{3-\delta}$ with 8YSZ and 20GDC. Solid State Ionics, 2006. **177**(13-14): p. 1199-1204.

[15] Leng, Y., Chan, C., Liu, Q. Development of LSCF–GDC composite cathodes for low-temperature solid oxide fuel cells with thin film GDC electrolyte. International Journal of Hydrogen Energy, 2008. **33**(14): p. 3808-3817.

[16] Fuel Cell Handbook, ed. I. EG&G Technical service. 2004, West Virginia: U.S. Department of Energy office of Fossil Energy.

[17] Joos, J. INSTITUTE OF MATERIALS FOR ELECTRICAL AND ELECTRONIC ENGINEERING. Available from: https://www.iwe.kit.edu/english/mitarbeiter_2599.php

[18] Taroco, H. A., Domingues, R. Z., Matencio, T. Advance in Ceramic. Synthesis and Characterization, Processing and Specific Applications ed. C. Sikalidis. InTech.

[19] Zhu, W.Z., Deevi, S.C. A review on the status of anode materials for solid oxide fuel cells. Materials Science and Engineering: A, 2003. **362**(1-2): p. 228-239.

[20] Sorrell, C, C., Sugihara, S. Materials for Energy Conversion Device. 2005, North America: Woodhead.

[21] Sun, C., Hui, R., Roller, J. Cathode materials for solid oxide fuel cells: a review. Journal of Solid State Electrochemistry, 2009. **14**(7): p. 1125-1144.

[22] Janardhanan, V.M., Heuveline, V., Deutshman, O. Three-phase boundary length in solid-oxide fuel cells: A mathematical model. Journal of Power Sources, 2008. **178**(1): p. 368-372.

[23] Richter, J., et al., Materials design for perovskite SOFC cathodes. Monatshefte für Chemie - Chemical Monthly, 2009. **140**(9): p. 985-999.

[24] Chroneos, A., et al., Oxygen transport in perovskite and related oxides: A brief review. Journal of Alloys and Compounds, 2010. **494**(1-2): p. 190-195.

[25] Sherman J. X. Oxygen permeation rates through ion-conducting perovskite membranes. Chemical Engineering Science, 1999. **54**: p. 3839-3850.

[26] Ruiz-Morales, C. J., Gálvez-Sánchez, M., Canales-Vázquez, J., Cristian, S., Stanislav, N. S. Engineering of materials for solid oxide fuel cells and other energy and environmental applications. Energy & Environmental Science, 2010. **3**(11): p. 1670-1681.

[27] Barsoukov, E. Impedance Spectroscopy, Theory Experiment and Applications - Macdonald. 2005, USA: John Wiley & Sons, Inc.

[28] Lin, Y., Beale, S.B. Performance predictions in solid oxide fuel cells. Applied Mathematical Modelling, 2006. **30**(11): p. 1485-1496.

[29] Wei, B., et al., Synthesis, electrical and electrochemical properties of $Ba_{0.5}Sr_{0.5}Zn_{0.2}Fe_{0.8}O_{3-\delta}$ perovskite oxide for IT-SOFC cathode. Journal of Power Sources, 2008. **176**(1): p. 1-8.

[30] Archimedes' principle and specific density. Available from: http://www.physics.arizona.edu/physics/gdresources/documents/13_Archimedes.

[31] Ratchaoun, C., PREPARATION OF $La_{2-x}Ca_xNi_{1-y}Co_y$(Ga, Ti)zO4 FOR SOLID OXIDE FUEL CELL, in Petrochemistry and Polymer Science2010, Chulalongkorn University.

[32] Ruengwranit, C., Electrocatalytic Activation for the Anodic Oxidation of Methane in Solid Oxide Fuel Cll based on the Ni-Co/CeO2-based Cermet, in Chemistry2010, Chulalongkorn University.

[33] Pascual, C., Duran, P. Electrical behaviour of doped-yttria stabilized zirconia ceramic materials,. Journal of Material Science, 1983.

[34] Kaliaguine, S. Neste, A. V. Process for synthesizing metal oxides and metal oxides having a perovskite or perovskite-like crystal structure, 2004, Google Patents.

[35] Harumi, Y., Teruhisa, H., Katsuhiko, Y., Yu-ping, X. ROLES OF CERIA IN SOFC ELECTRODE. Fuel Chemistry Division Preprints. **47**(1): p. 501-502.

[36] Ying, L., Chang-Zhen, W. Preparation and Properties of $CaZr_{1-x}In_xO_{3-\delta}$;Proton Conductor. Journal of Inorganic Materials, 2012. **27**(4): p. 427-432.

[37] Handcock, C.A., Varcoe, J.R., Slater, P.R. Synthesis, structure and conductivity of sulfate and phosphate doped $SrCoO_3$.

[38] Kenji, S., Motohide, M., Yoko, S. Preparation of yttria-stabilized zirconia fibers from a zirconia sol and their properties. Journal of the Ceramic Society of Japan, 2012. **120**(11): p. 478-482

[39] Mustapha, M., Ismail, F., Mamat, O. Empirical Relationship between Relative Electrical Conductivity and Relative Density of the Al-Foam Fabricated through Pressure Assisted Sintering/Dissolution Process. IOP Conference Series: Materials Science and Engineering, 2011. **17**: p. 012014.

[40] Materials for Energy Conversion Devices. 1st ed. 2005: Woodhead Publishing.

[41] Leonide, A. SOFC modelling and parameter identification by means of impedance spectroscopy. 2010, Karlsruhe: KIT Scientific Plublishing.

APPENDIX

APPENDIX A

A-1. XRD patterns of $(Ba_{0.5}Sr_{0.5})_{0.7}Ca_{0.3}Co_{0.8}Fe_{0.2}O_{3-\delta}$-YSZ composite (BSCCF: YSZ)

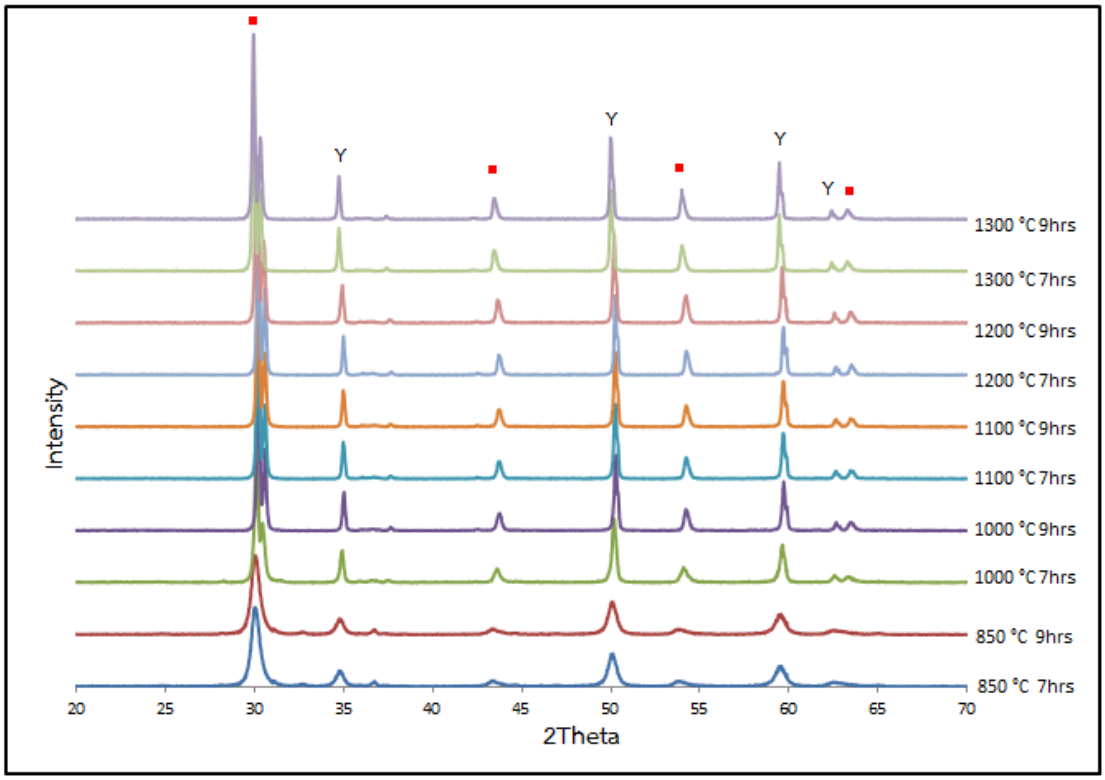

Figure A-1.1 XRD patterns of $(Ba_{0.5}Sr_{0.5})_{0.7}Ca_{0.3}Co_{0.8}Fe_{0.2}O_{3-\delta}$-YSZ composite in weight ratio of 1:3 (BSCCF:YSZ) calcined at 1000 – 1300°C for 7 -9 hrs, (YSZ (Y), $Sr(ZrO_3)$ (■))

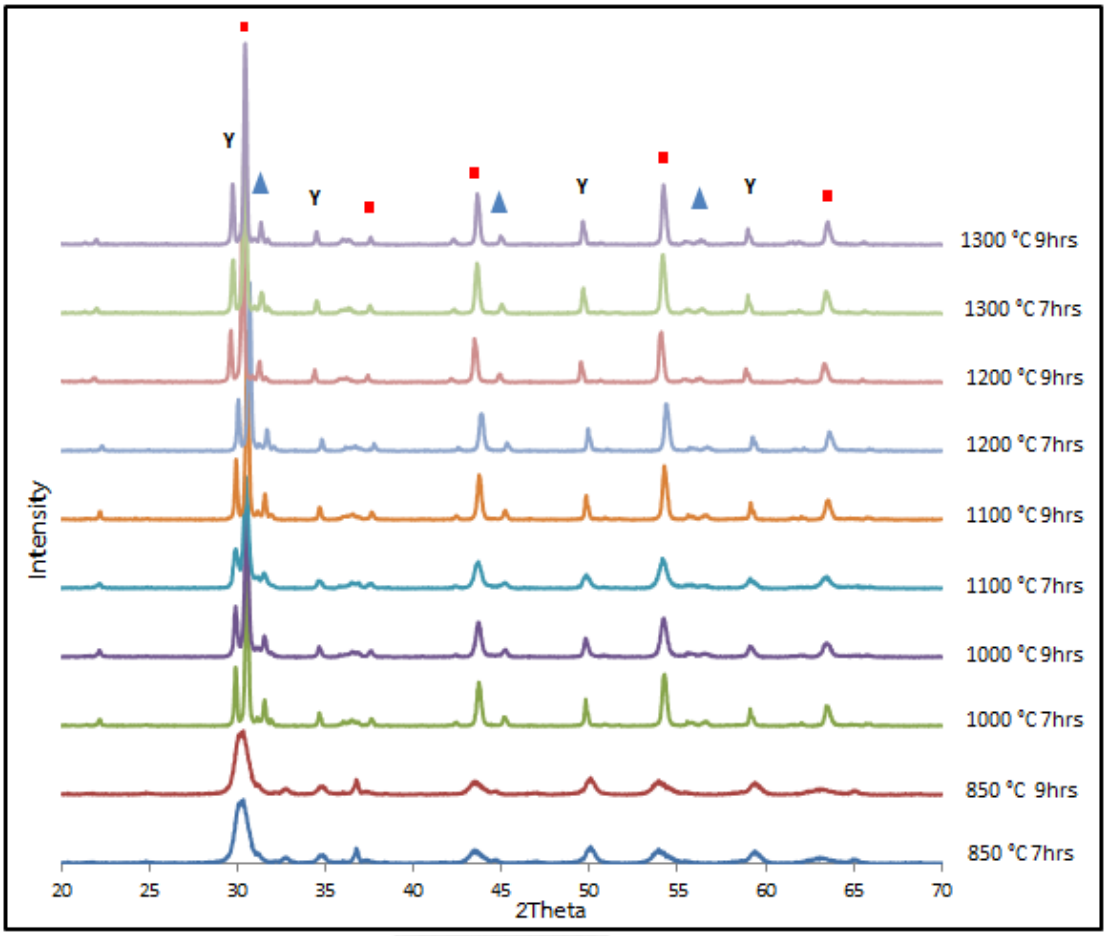

Figure A-1.2 XRD patterns of $(Ba_{0.5}Sr_{0.5})_{0.7}Ca_{0.3}Co_{0.8}Fe_{0.2}O_{3-\delta}$-YSZ composite in weight ratio of 1:1 (BSCCF:YSZ) calcined at 850 – 1300°C for 7-9 hrs.
(YSZ(Y), $Sr(ZrO_3)$(■), $CaZrO_3$(▲))

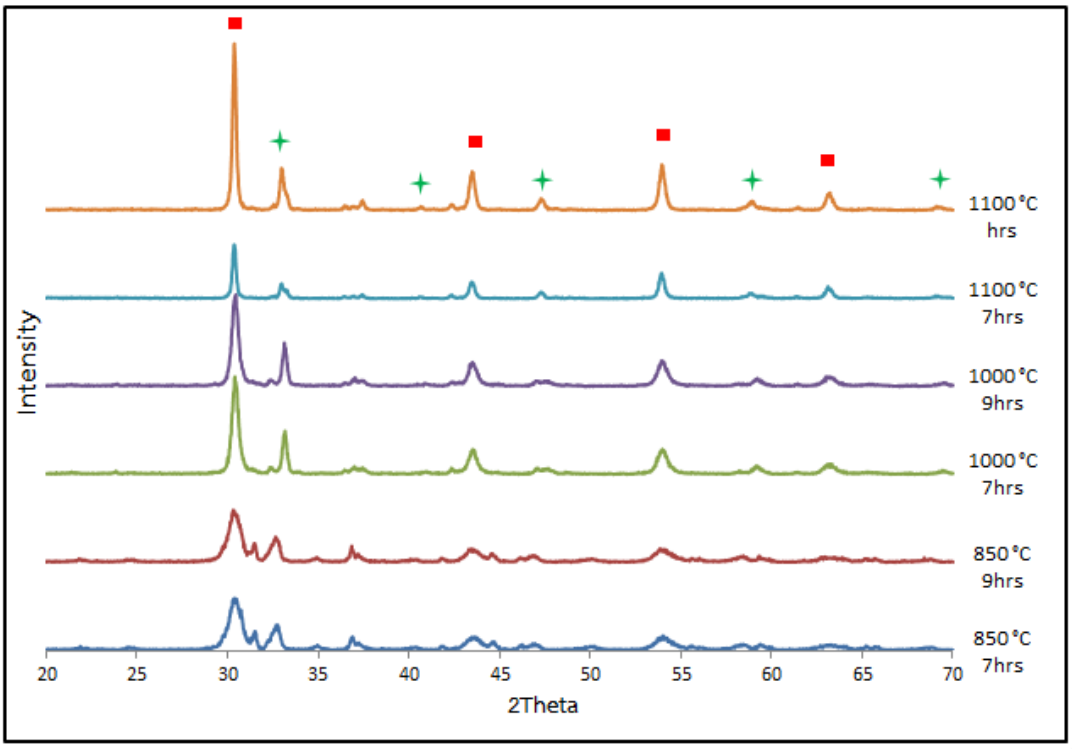

Figure A-1.3 XRD patterns of $(Ba_{0.5}Sr_{0.5})_{0.7}Ca_{0.3}Co_{0.8}Fe_{0.2}O_{3-\delta}$-YSZ composite in weight ratio of 3:1 (BSCCF:YSZ) calcined at 850 – 1100°C for 7-9 hrs.

(BSCCF (P), YSZ(Y), $Sr(ZrO_3)$(■), $SrCoO_3$(✦)

A-2. XRD patterns of $(Ba_{0.5}Sr_{0.5})_{0.7}Ca_{0.3}Co_{0.8}Fe_{0.2}O_{3-\delta}$-GDC composite (BSCCF:GDC)

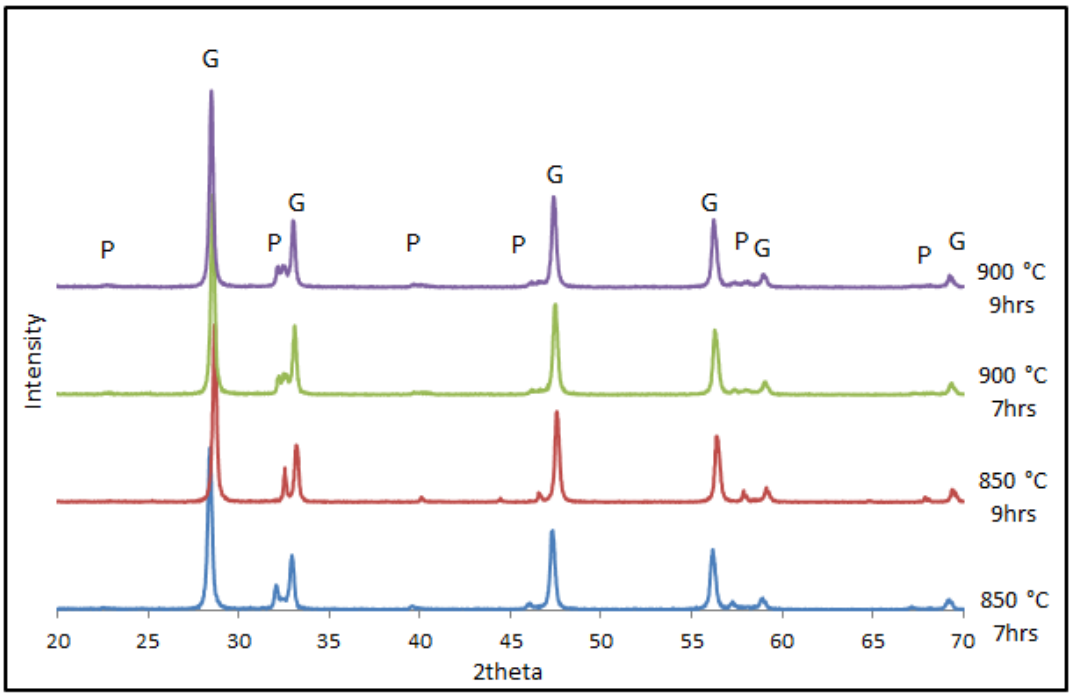

Figure A-2.1 XRD patterns of mixed powder of BSCCF and GDC in weight ratio of 1:3 (BSCCF:GDC) calcined at 850-900 °C for 7-9 hrs. (BSCCF (P), GDC (G)

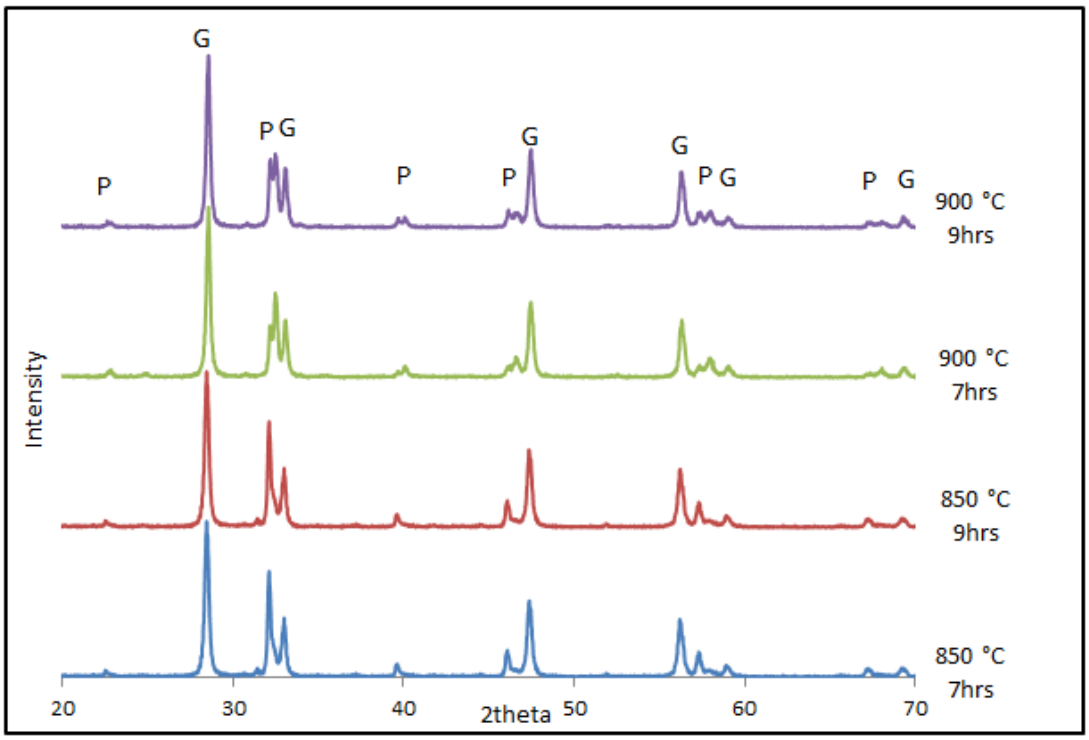

Figure A-2.2 XRD patterns of mixed powder of BSCCF and GDC in weight ratio of 1:1 (BSCCF:GDC) calcined at 850-900 °C for 7-9 hrs. (BSCCF (P), GDC (G)

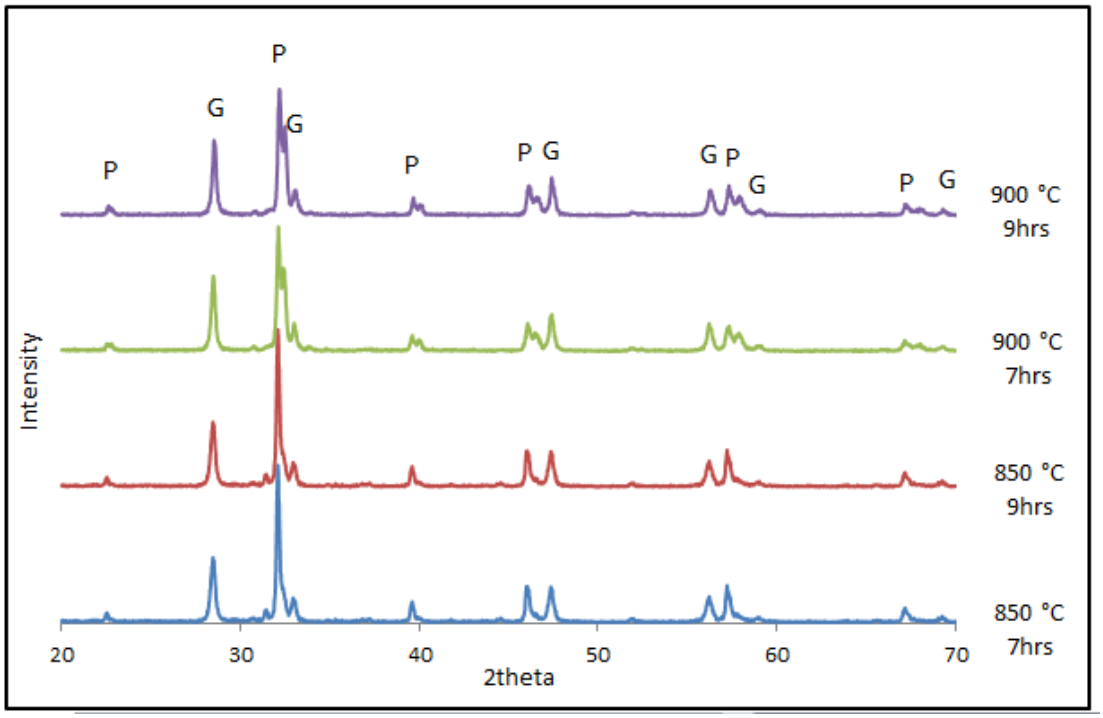

Figure A-2.3 XRD patterns of mixed powder of BSCCF and GDC in weight ratio of 3:1 (BSCCF:GDC) calcined at 850-900 °C for 7-9 hrs. (BSCCF (P), GDC (G)

APPENDIX B

B-1. Activation energy (E_a)

Arrhenius Equation is used to determine the activation energy (E_a)

From Equation

$$R_p^{-1} = Ae^{(-Ea/RT)}$$

$$\ln R_p^{-1} = \ln A + \ln e^{(-Ea/RT)}$$

$$\ln R_p^{-1} = \ln A - (Ea/RT) \ln e$$

$$\ln R_p^{-1} = \ln A - (Ea/RT)$$

$$\ln R_p^{-1} = -(Ea/R)(1/T) + \ln A \quad [y = mx + b]$$

VITA

Miss Wichuma Jiraroj was born on October 31, 1987 in Bangkok, Thailand. She graduated with Bachelor's Degree of Chemistry from Faculty of Science, Chulalongkorn University in 2009 . She continued her study in program of Chemistry, Faculty of Science, Chulalongkorn University in 2010 and completed in 2013.